PHYSICAL REVIEW D 92, 095025 (2015)

Simple non-Abelian extensions of the standard model gauge group and the diboson excesses at the LHC

Qing-Hong Cao,[1,2,3,*] Bin Yan,[1,†] and Dong-Ming Zhang[1,‡]
[1]Department of Physics and State Key Laboratory of Nuclear Physics and Technology, Peking University, Beijing 100871, China
[2]Collaborative Innovation Center of Quantum Matter, Beijing 100871, China
[3]Center for High Energy Physics, Peking University, Beijing 100871, China
(Received 25 July 2015; published 23 November 2015)

The ATLAS collaboration reported excesses at around 2 TeV in the diboson production decaying into hadronic final states. We consider the possibility of explaining the excesses with extra gauge bosons in two simple non-Abelian extensions of the standard model. One is the so-called $G(221)$ models with a symmetry structure of $SU(2)_1 \otimes SU(2)_2 \otimes U(1)_X$ and the other is the $G(331)$ models with an extended symmetry of $SU(3)_C \otimes SU(3)_L \otimes U(1)_X$. The W' and Z' bosons emerge after the electroweak symmetry is spontaneously broken. Two patterns of symmetry breaking in the $G(221)$ models are considered in this work: one is $SU(2)_L \otimes SU(2)_2 \otimes U(1)_X \to SU(2)_L \otimes U(1)_Y$, the other is $SU(2)_1 \otimes SU(2)_2 \otimes U(1)_Y \to SU(2)_L \otimes U(1)_Y$. The symmetry breaking of the $G(331)$ model is $SU(3)_L \otimes U(1)_X \to SU(2)_L \otimes U(1)_Y$. We perform a global analysis of W' and Z' phenomenology in ten new physics models, including all the channels of W'/Z' decay. Our study shows that the leptonic mode and the dijet mode of W'/Z' decays impose a very stringent bound on the parameter space in several new physics models. Such tight bounds provide a useful guide for building new physics models to address on the diboson anomalies. We also note that the left-right and leptophobic models can explain the $3.4\sigma WZ$ excess if the 2.6σ deviation in the W^+W^- pair around 2 TeV were confirmed to be a fluctuation of the SM backgrounds.

DOI: 10.1103/PhysRevD.92.095025 PACS numbers: 12.60.Cn, 12.60.-i, 14.70.Pw

I. INTRODUCITON

Searches for new physics (NP) effects in the final state of vector boson pairs have been carried out recently by both ATLAS [1] and CMS [2,3] collaborations using the technique of jet substructure. It was reported recently by the ATLAS collaboration [1] that, using a data sample with 20 fb^{-1} integrated luminosity, a 3.6σ deviation is observed in the invariant mass distribution of the WZ pair, which requires a NP contribution to the cross section of the WZ production as $\sigma(WZ) \sim 4$–8 fb. Also a 2.6σ and 2.9σ deviation is observed in the invariant mass distribution of WW and ZZ pair production, respectively. The NP contributions of $\sigma(WW) \sim 3$–7 fb and $\sigma(ZZ) \sim 3$–9 fb are needed to explain the excesses. All the three excesses occur around 2 TeV in the invariant mass distribution of vector boson pair.[1] The vector boson pair production is highly correlated with the associated production of a vector boson and Higgs boson. The CMS collaboration has obtained a bound on the cross section of WH and ZH productions [4], $\sigma(WH) \leq 7.1$ fb and $\sigma(ZH) \leq 6.8$ fb, respectively.

As the final state involves two gauge bosons, it is natural to consider the excesses are induced by a spin-one resonances in new physics (NP) beyond the SM. Those heavy gauge bosons might arise from an extension of the SM with additional non-Abelian gauge symmetry. It is interesting to ask whether or not the deviation can be addressed by heavy gauge bosons after one takes into account other precision data. There has been recent excitement among theorists for this measurement at the LHC [5–13].

In this work we consider two kinds of non-Abelian gauge extension to the SM: one is the so-called $G(221)$ models with a symmetry of $SU(2)_1 \otimes SU(2)_2 \otimes U(1)_X$ [14–16] and the other is the $G(331)$ model with a symmetry of $SU(3)_C \otimes SU(3)_L \otimes U(1)_X$ [17,18]. Both charged extra boson W' and new neutral boson Z' arise after the symmetry breaking. Several $G(221)$ and $G(331)$ models are examined in this work. We demonstrate that the leptonic decay and dijet decay modes of W'/Z' impose a very stringent bound on the parameter space of those NP models. In order to explain the WW/WZ excess under the two simple extensions, the leptonic and dijet decay modes of those extra gauge bosons need to be largely reduced in a more complete NP theory.

There are a few bounds from the W'/Z' searches in their fermionic decays at the LHC, e.g., for a 2 TeV W'/Z',

*qinghongcao@pku.edu.cn
†binyan@pku.edu.cn
‡zhangdongming@pku.edu.cn

[1]The CMS collaboration also performed similar searches in the diboson channel [2,3] but no excess was observed. In this study we focus on the ATLAS results and explore the NP explanation of those diboson excesses.

TABLE I. The charge assignments of the SM fermions under the $G(221)$ gauge groups. Unless otherwise specified, the charge assignments apply to all three generations.

Model	$SU(2)_1$	$SU(2)_2$	$U(1)_X$
Left-right (LR)	$\begin{pmatrix} u_L \\ d_L \end{pmatrix}, \begin{pmatrix} \nu_L \\ e_L \end{pmatrix}$	$\begin{pmatrix} u_R \\ d_R \end{pmatrix}, \begin{pmatrix} \nu_R \\ e_R \end{pmatrix}$	$\frac{1}{6}$ for quarks, $-\frac{1}{2}$ for leptons
Leptophobic (LP)	$\begin{pmatrix} u_L \\ d_L \end{pmatrix}, \begin{pmatrix} \nu_L \\ e_L \end{pmatrix}$	$\begin{pmatrix} u_R \\ d_R \end{pmatrix}$	$\frac{1}{6}$ for quarks, $Y_{\rm SM}$ for leptons
Hadrophobic (HP)	$\begin{pmatrix} u_L \\ d_L \end{pmatrix}, \begin{pmatrix} \nu_L \\ e_L \end{pmatrix}$	$\begin{pmatrix} \nu_R \\ e_R \end{pmatrix}$	$Y_{\rm SM}$ for quarks, $-\frac{1}{2}$ for leptons
Fermiophobic (FP)	$\begin{pmatrix} u_L \\ d_L \end{pmatrix}, \begin{pmatrix} \nu_L \\ e_L \end{pmatrix}$		$Y_{\rm SM}$ for all fermions
Un-unified (UU)	$\begin{pmatrix} u_R \\ d_R \end{pmatrix}$	$\begin{pmatrix} \nu_R \\ e_R \end{pmatrix}$	$Y_{\rm SM}$ for all fermions
Nonuniversal (NU)	$\begin{pmatrix} u_R \\ d_R \end{pmatrix}_{1^{\rm st},2^{\rm nd}}, \begin{pmatrix} \nu_R \\ e_R \end{pmatrix}_{1^{\rm st},2^{\rm nd}}$	$\begin{pmatrix} u_L \\ d_L \end{pmatrix}_{3^{\rm rd}}, \begin{pmatrix} \nu_L \\ e_L \end{pmatrix}_{3^{\rm rd}}$	$Y_{\rm SM}$ for all fermions

$\sigma(pp\to Z'/W'\to jj)\leq 102\,{\rm fb}$ [19,20], $\sigma(pp\to Z'\to t\bar{t})\leq 11$ fb [21], $\sigma(pp\to W'_R\to t\bar{b})\leq 124\,{\rm fb}$, $\sigma(pp\to W'_L\to t\bar{b})\leq 162\,{\rm fb}$ [22], $\sigma(pp\to Z'\to e^+e^-/\mu^+\mu^-)\leq 0.2$ fb [23,24] and $\sigma(pp\to W'\to e\nu/\mu\nu)\leq 0.7\,{\rm fb}$ [25,26]. We also take all the above bounds into account and perform a global analysis on each individual NP model.

It is hard to explain the ZZ excess in the simple non-Abelian gauge extension of the SM. The difficulty has been discussed extensively in Refs. [7,8,11]. For example, having an extra neutral gauge boson decaying to the ZZ mode would require the violation in P or CP symmetry 7]]. An alternative way is to introduce an extra scalar which predominately decays into ZZ and WW pairs. Unfortunately, the cross section of the scalar production is usually too tiny to explain the ZZ excess [8]. Therefore, we focus our attention on the WW and WZ excesses in this work.

The paper is organized as follows. In Sec. II we briefly review the $G(221)$ models. In Sec. III we present the NLO cross section of W'/Z' production at the LHC Run-1 and the PDF uncertainties. In Sec. IV we focus our attention on the first breaking pattern of $G(221)$ and discuss the left-right, leptophobic, hadrophobic and fermiophobic models. In Sec. V we study the second breaking pattern of $G(221)$ and explore the phenomenology of the un-unified and nonuniversal models. In Sec. VI we study the $G(331)$ model. Finally we conclude in Sec. VII.

II. $G(221)$ MODELS

The $G(221)$ model is the minimal extension of the SM, which consists of both W' and Z', exhibits a gauge structure of $SU(2)_1\otimes SU(2)_2\otimes U(1)_X$, named as $G(221)$ model [14,27–43]. The model can be viewed as the low energy effective theory of many NP models with extended gauge structure when all the heavy particles other than the W' and Z' bosons decouple. In particular, we consider several $G(221)$ models categorized as follows: left-right (LR) [27–29,44], lepto-phobibc (LP), hadron-phobic (HP), fermio-phobic (FP) [30,31,38], un-unified (UU) [32,33] and nonuniversal (NU) [34–36,39]. The charge assignments of the SM fermion in those models are listed in Table I.

We classify the $G(221)$ models based on the pattern of symmetry breaking and quantum number assignment of the SM fermions. The symmetry breaking is assumed to be induced by fundamental scalar fields whose quantum number under the $G(221)$ gauge group depends on the breaking pattern. The NP models mentioned above fall into the following two patterns of symmetry breaking:

(i) breaking pattern I (BP-I):
$SU(2)_1$ is identified as the $SU(2)_L$ of the SM. The first stage of symmetry breaking $SU(2)_2\times U(1)_X\to U(1)_Y$ occurs at the TeV scale, while the second stage of symmetry breaking $SU(2)_L\times U(1)_Y\to U(1)_{\rm em}$ takes place at the electroweak scale;

(ii) breaking pattern II (BP-II):
$U(1)_X$ is identified as the $U(1)_Y$ of the SM. The first stage of symmetry breaking $SU(2)_1\times SU(2)_2\to SU(2)_L$ occurs at the TeV scale, while the second stage of symmetry breaking $SU(2)_L\times U(1)_Y\to U(1)_{\rm em}$ happens at the electroweak scale.

The W' and Z' arise after the symmetry breaking at the TeV scale. The most general interaction of the Z' and W' to SM fermions is

$$\mathcal{L}_f = Z'_\mu\bar{f}\gamma^\mu(g_L P_L + g_R P_R)f + W'_\mu\bar{f}\gamma^\mu(g'_L P_L + g'_R P_R)f' + {\rm H.c.}, \tag{1}$$

where $P_{L,R}=(1\mp\gamma_5)/2$ are the usual chirality projectors. For simplicity, we use g_L and g_R for both Z' and W' bosons from now on. Note that throughout this work only SM fermions are considered, despite in certain models new heavy fermions are necessary to cancel gauge anomalies.

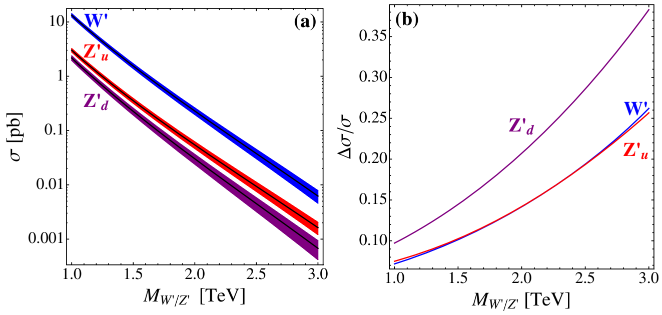

FIG. 1 (color online). The NLO cross section of $pp \to W'/Z'$ with a sequential coupling as a function of $M_{W'/Z'}$ calculated with the CT14 NNLO PDFs at LHC Run-1. (a) The PDF uncertainty bands and (b) the relative PDF uncertainties $\Delta\sigma/\sigma$ of $\sigma_{W'}$ and $\sigma^u_{Z'}$ and $\sigma^d_{Z'}$, where $\sigma^u_{Z'}$ and $\sigma^d_{Z'}$ represent the cross sections induced by up-type and down-type quark initial states, respectively.

III. THE W'/Z' PRODUCTION CROSS SECTION

The W' and Z' are produced singly through the Drell-Yan process. Following the experimental searches, we adapt the narrow width approximation (NWA) to factorize the process of $pp \to W'/Z' \to V_1V_2$ as follows:

$$\sigma(pp \to V' \to XY) \simeq \sigma(pp \to V') \otimes \mathrm{BR}(V' \to XY) \equiv \sigma(V') \times \mathrm{BR}(V' \to XY), \quad (2)$$

where X and Y denote the decay products of the V' boson. Next we consider a few $G(221)$ models and discuss their implications on the VV' and VH productions.

An accurate theory prediction of the cross section of W' and Z' productions is crucial for disentangling the NP signal from the SM backgrounds. We calculate the quantum chromodynamics (QCD) corrections to cross section of a sequential W'/Z' boson production at the next-to-leading-order (NLO). For simplicity we set the renormalization scale (μ_R) and the factorization scale (μ_F) to be equal. The cross section exhibits two theoretical uncertainties: one is from the parton distribution function (PDF), the other is from the choice of $\mu = \mu_R = \mu_F$. In this work we adapt the CT14 NNLO PDFs [45] to calculate the NLO QCD corrections to the cross section of a sequential W'/Z' boson production $\sigma(W'/Z')$. The 57 sets of the CT14 NNLO PDFs are used to evaluate the PDF uncertainties. Figure 1 displays $\sigma(W'/Z')$ as a function of $M_{W'/Z'}$. The default renormalization and factorization scales are chosen as the mass of extra gauge bosons $\mu_R = \mu_F = M_{W'/Z'}$. As a rule of thumb, we vary the scale μ by a factor of 2 to estimate the higher order corrections. The scale uncertainties are about 5% in the W' and Z' production, which are found to be much smaller than the PDF uncertainties. We thus focus on the PDF uncertainties of $\sigma(W'/Z')$. Figure 1(a) shows the NLO cross section of $pp \to W'/Z'$ and the corresponding PDF uncertainties denoted by the shaded band as a function of $M_{W'/Z'}$ at the LHC Run-1. In order to model the NP effects, we treat the up-type quark and down-type quark initial states separately in the Z' production; see the Z'_u and Z'_d bands. The relative uncertainties of PDFs are plotted in Fig. 1(b), which shows the uncertainties are about 10% for $M_{W'/Z'} \sim$ TeV and 30% for $M_{W'/Z'} \sim 3$ TeV. Following Ref. [46], we fit the theory prediction of the cross section by a simple three parameter analytic expression,

$$\log\left[\frac{\sigma(M_{V'})}{\mathrm{pb}}\right] = A\left(\frac{M_{V'}}{\mathrm{TeV}}\right)^{-1} + B + C\left(\frac{M_{V'}}{\mathrm{TeV}}\right), \quad (3)$$

where $V' = W'/Z'$. The cross sections are normalized to picobarn (pb) while $M_{W'/Z'}$ to TeV. The fitting functions of the production cross sections of W' and Z' are

$$\begin{aligned} W'&: 4.59925 + 1.34518x^{-1} - 3.37137x \\ Z'_u&: 2.82225 + 1.51681x^{-1} - 3.24437x \\ Z'_d&: 2.88763 + 1.42266x^{-1} - 3.54818x, \end{aligned} \quad (4)$$

where $x = M_{W'/Z'}/\mathrm{TeV}$.

To explain the diboson excess of the ATLAS collaboration results, we consider a 2 TeV W'/Z' boson in this work. The production cross sections of a sequential W'/Z' boson at the LHC Run-1 are

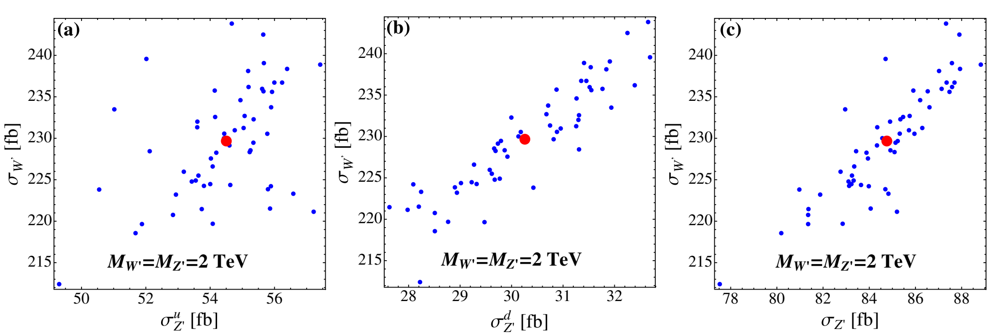

FIG. 2 (color online). $\sigma_{W'}$ versus $\sigma_{Z'_u}$ (a), $\sigma_{Z'_d}$ (b) and $\sigma_{Z'}$ (c) for $M_{W'} = M_{Z'} = 2$ TeV. The blue point represents the cross sections calculated with 56 sets of PDFs while the red spot label the cross section evaluated with the central PDF.

$$\sigma^{SQ}_{W'} = 229.67 \pm 32.54(\mathrm{PDF})^{+12.54}_{-12.49}\ \mathrm{fb(scale)},$$
$$\sigma^{SQ}_{Z'u} = 54.50 \pm 7.74(\mathrm{PDF})^{+2.87}_{-2.86}\ \mathrm{fb(scale)},$$
$$\sigma^{SQ}_{Z'd} = 30.25 \pm 6.27(\mathrm{PDF})^{+1.71}_{-1.71}\ \mathrm{fb(scale)}. \quad (5)$$

The PDF uncertainties are $\sim 14\%$ for both $\sigma(W')$ and $\sigma(Z'_u)$ while it is $\sim 21\%$ for $\sigma(Z'_d)$. Using CT10 NLO PDFs [47] slightly increases the PDF uncertainties. For example, the uncertainty of $\sigma(W')$ and $\sigma(Z'_u)$ are $\sim 17\%$ and that of $\sigma(Z'_d)$ is about 24%. In this work we choose the benchmark points shown in Eq. (5) as a reference to calculate the production cross sections of W' and Z' in several NP models.

As the W' and Z' are correlated in NP models with non-Abelian extension gauge structures, we explore the correlation between $\sigma(W')$ and $\sigma(Z'_{u,d})$ for the 56 sets of CT14 NNLO PDFs. Figure 2 displays $\sigma(W')$ versus $\sigma(Z'_u)$ (a) and $\sigma(Z'_d)$ (b) at the LHC Run-1. The red point represents the cross section from the PDF set which the global fitting variables with central values, while the blue points denote the cross section from other PDF sets. The 56 PDF sets yield a correlation between $\sigma(W')$ and $\sigma(Z'_d)$. On the other hand, the correlation is diluted in $\sigma(W')$ versus $\sigma(Z'_u)$. In Fig. 2(c) we plot the production cross sections of the sequential W' and Z' boson, which exhibit a linear correlation.

IV. $G(211)$ MODELS: BREAKING PATTERN I

We first consider several NP models exhibiting the first type symmetry breaking pattern. In the BP-I, $SU(2)_1$ is identified as the $SU(2)_L$ of the SM. The first stage of symmetry breaking $SU(2)_2 \times U(1)_X \to U(1)_Y$ occurs at the TeV scale, which could be induced by a scalar doublet field $\Phi \sim (1, 2, 1/2)$, or a triplet scalar field $\Sigma \sim (1, 3, 1)$ with a vacuum expectation value (VEV) u. The explicit form of the doublet and triplet as well as their vacuum expectation values are given as follows:

$$\Phi = \begin{pmatrix} \phi^+ \\ \phi^0 \end{pmatrix}, \qquad \langle\Phi\rangle = \frac{1}{\sqrt{2}}\begin{pmatrix} 0 \\ u \end{pmatrix},$$
$$\Sigma = \frac{1}{\sqrt{2}}\begin{pmatrix} \phi^+ & \sqrt{2}\phi^{++} \\ \sqrt{2}\phi^0 & -\phi^+ \end{pmatrix}, \qquad \langle\Sigma\rangle = \frac{1}{\sqrt{2}}\begin{pmatrix} 0 & 0 \\ u & 0 \end{pmatrix}. \quad (6)$$

The second stage of symmetry breaking $SU(2)_L \times U(1)_Y \to U(1)_{\mathrm{em}}$ takes place at the electroweak scale. It is via another scalar field $H \sim (2, \bar{2}, 0)$ with two VEVs v_1 and v_2, which can be redefined as a VEV $v = \sqrt{v_1^2 + v_2^2}$ and a mixing angle $\beta \equiv \arctan(v_1/v_2)$. The detailed form of H and its VEV are

$$H = \begin{pmatrix} h_1^0 & h_1^+ \\ h_2^- & h_2^0 \end{pmatrix}, \qquad \langle H\rangle = \frac{1}{\sqrt{2}}\begin{pmatrix} v_1 & 0 \\ 0 & v_2 \end{pmatrix}. \quad (7)$$

We denote g_1, g_2, and g_X as the coupling of $SU(2)_1$, $SU(2)_2$, and $U(1)_X$, respectively. In the BP-I, the three couplings are

$$g_1 = \frac{e}{s_W}, \qquad g_2 = \frac{e}{c_W s_\phi}, \qquad g_X = \frac{e}{c_W c_\phi}, \quad (8)$$

where s_W and c_W are sine and cosine of the SM weak mixing angle, while s_ϕ and c_ϕ are sine and cosine of the new mixing angle $\phi \equiv \arctan(g_X/g_2)$ appearing after the TeV symmetry breaking. After symmetry breaking both W' and Z' bosons obtain masses and mix with the SM gauge bosons. Different electroweak symmetry breaking (EWSB) patterns will induce different W' and Z' mass relations. When the first stage breaking of BP-I is realized by the doublet Φ, the masses of the W' and Z' are

$$M^2_{W'^\pm} = \frac{e^2 v^2}{4 c_W^2 s_\phi^2}(x+1), \qquad M^2_{Z'} = \frac{e^2 v^2}{4 c_W^2 s_\phi^2 c_\phi^2}(x + c_\phi^4), \quad (9)$$

where $x = u^2/v^2$. Note that the precision data constraints (including those from CERN LEP and SLAC SLC experiment data) pushed the TeV symmetry breaking higher than 1 TeV. Therefore, we assume x is much larger than 1 and approximate the predictions of physical observables by taking Taylor expansion in $1/x$. As a result, the masses of W' and Z' are almost degenerated in the region of $c_\phi \sim 1$.

If the symmetry breaking is realized by the triplet Σ, the Z' mass is much larger than the W' mass

$$M^2_{W'^\pm} = \frac{e^2 v^2}{4 c_W^2 s_\phi^2}(2x+1), \qquad M^2_{Z'} = \frac{e^2 v^2}{4 c_W^2 s_\phi^2 c_\phi^2}(4x + c_\phi^4). \quad (10)$$

The recent discovered excesses occur around $M_{W'} \simeq M_{Z'} \sim 2$ TeV [1]. That leads us to focus on the doublet model throughout this work. The triplet model is studied in Ref. [11].

After the second stage of symmetry breaking at the electroweak scale, a non-Abelian coupling of the W' and Z' to the SM bosons are generated as follows:

$$HW_\nu W'_\rho:\ -\frac{1}{2}\frac{e^2 s_{2\beta}}{c_W s_W s_\phi} v g_{\nu\rho}\left[1 + \frac{(c_W^2 s_\phi^2 - s_W^2)}{x s_W^2}\right],$$
$$HZ_\nu Z'_\rho:\ -\frac{1}{2}\frac{e^2 c_\phi}{c_W^2 s_W s_\phi} v g_{\nu\rho}\left[1 - \frac{c_\phi^2(c_\phi^2 s_W^2 - s_\phi^2)}{x s_W^2}\right],$$
$$W^+_\mu W'^-_\nu Z_\rho:\ \frac{e s_{2\beta} s_\phi}{x s_W^2},$$
$$W^+_\mu W^-_\nu Z'_\rho:\ \frac{e s_\phi c_W c_\phi^3}{x s_W^2}, \quad (11)$$

where the Lorentz index $[g^{\mu\nu}(k_1 - k_2)^\rho + g^{\nu\rho}(k_2 - k_3)^\mu + g^{\rho\mu}(k_3 - k_1)^\nu]$ in the three gauge boson couplings is implied.

The detailed expressions of the partial decay widths of W'/Z' are listed in the Appendix. The equivalence theorem tells us that one can treat the final state vector bosons as Nambu-Goldstone bosons in the high energy limit. We compare the bosonic decay of W'/Z' in the limit of $x \gg 1$ and $M_{W'/Z'} \gg m_{W/Z/H}$ and verify in the BP-I that

$$\frac{\mathrm{BR}(W' \to WZ)}{\mathrm{BR}(W' \to WH)} \sim 1, \qquad \frac{\mathrm{BR}(Z' \to WW)}{\mathrm{BR}(Z' \to ZH)} \sim 1. \tag{12}$$

It is worth mentioning that the WH mode might be suppressed in an UV completion model which exhibits a rather complicated scalar potential.

The couplings of the W' bosons to the SM fermions in the notation in Eq. (1) are

$$g_L^{W'\bar{f}f'} = -\frac{e}{\sqrt{2}s_W^2}\gamma_\mu \frac{c_W s_{2\beta} s_\phi}{x},$$
$$g_R^{W'\bar{f}f'} = \frac{e}{\sqrt{2}c_W s_\phi}\gamma_\mu, \tag{13}$$

while those of the Z' boson are

$$g_L^{Z'\bar{f}f} = \frac{e}{c_W c_\phi s_\phi}\gamma_\mu \left[(T_3^1 - Q)s_\phi^2 - \frac{c_\phi^4 s_\phi^2 (T_3^1 - Q s_W^2)}{x s_W^2}\right],$$
$$g_R^{Z'\bar{f}f} = \frac{e}{c_W c_\phi s_\phi}\gamma_\mu \left[(T_3^2 - Q s_\phi^2) + Q\frac{c_\phi^4 s_\phi^2}{x}\right], \tag{14}$$

where T_3^1 and T_3^2 are the third components of the generator of gauge groups $SU(2)_1$ and $SU(2)_2$, and Q is the electric charge of fermion f.

Next we consider specific NP models and discuss their implications in the production of W'/Z' and their decay modes of the WZ/WW pair at the LHC.

A. Left-right doublet model

1. The W' constraints

We begin with the left-right model in which the left-handed and right-handed fermion doublets are gauged under $SU(2)_1$ and $SU(2)_2$, respectively. Figure 3 displays the contour of the total width $\Gamma_{W'}$ and the ratio $\Gamma_{W'}/M_{W'}$ in the plane of c_ϕ and $s_{2\beta}$. It is clear that $\Gamma_{W'} \ll M_{W'}$ in all of the parameter space such that it is reasonable to factorize the $\sigma(pp \to V' \to V_1 V_2) \equiv \sigma(V') \times \mathrm{BR}(V' \to V_1 V_2)$. The ratio $\Gamma_{W'}/M_{W'}$ depends on c_ϕ mildly but it is not sensitive to $s_{2\beta}$. Note that $s_{2\beta}$ appears only in the left-handed couplings of W' to the SM fermions which is suppressed by x. On the other hand, the right-handed coupling of W' depends only on c_ϕ.

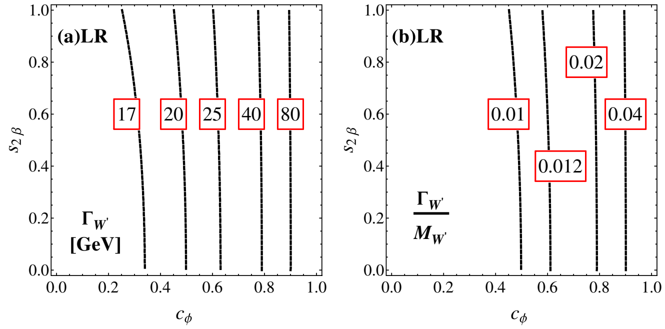

FIG. 3 (color online). The contours of the total width of W' (a) and the ratio of total width and mass of W' (b) in the plane of c_ϕ and $s_{2\beta}$ in the left-right model.

Figure 4(a) displays the contour of the cross section of $\sigma(W') \times \mathrm{BR}(W' \to WZ)$ in the plane of c_ϕ and $s_{2\beta}$. The yellow bands represent the degenerated region of $M_{W'}$ and $M_{Z'}$. In order to produce $\sigma(WZ) \sim 4$–8 fb and $\sigma(W') \times \mathrm{BR}(W' \to jj) \leq 102$ fb [20], one needs $0.73 < c_\phi < 0.75$ and $s_{2\beta} \gtrsim 0.9$.

In accord to the equivalence theorem, the vector-boson pair production is highly correlated with the associated production of the vector boson and Higgs boson. We also plot in Fig. 4(b) the contour of the cross section of $\sigma(W') \times \mathrm{BR}(W' \to WH)$ in the plane of c_ϕ and $s_{2\beta}$. In the

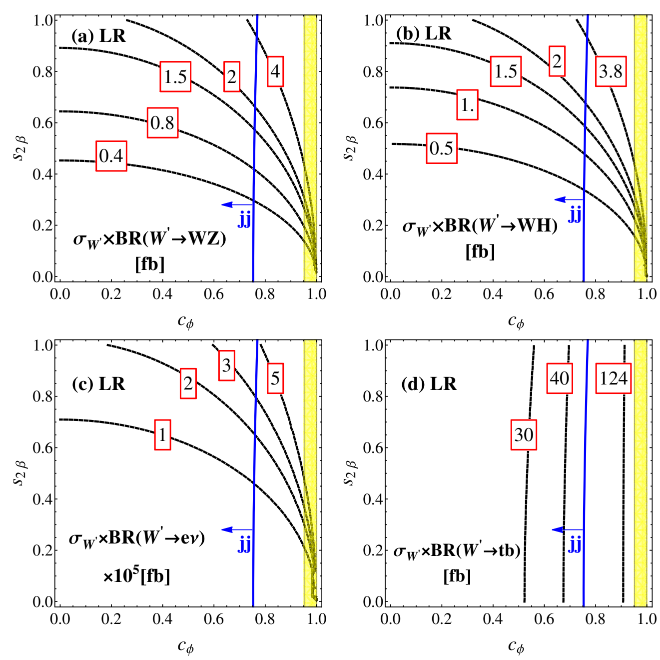

FIG. 4 (color online). The contours of the cross section (a) $\sigma(W') \times \mathrm{BR}(W' \to WZ)$, (b) $\sigma(W') \times \mathrm{BR}(W' \to WH)$, (c) $\sigma(W') \times \mathrm{BR}(W' \to e\nu)$ and (d) $\sigma(W') \times \mathrm{BR}(W' \to tb)$ in the plane of c_ϕ and $s_{2\beta}$. The vertical line (jj) denotes the constraint from the di-jet measurements. The yellow band represents the degenerated mass region of W' and Z'.

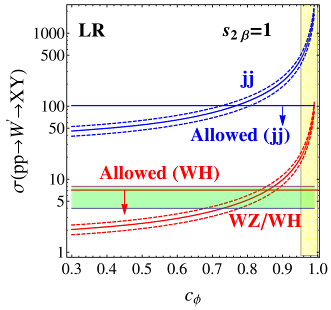

FIG. 5 (color online). The cross section of $pp \to W' \to WZ/WH$ (red curves) and $pp \to W' \to jj$ (blue curves) as a function of c_ϕ with $s_{2\beta} = 1$. The dashed curves represent the PDF uncertainties. The green shaded region represents the parameter space compatible with the WZ excess. The yellow shaded region is required for $M_{W'} \simeq M_{Z'}$. The current experimental limits of $\sigma(pp \to W' \to jj) < 102$ fb and $\sigma(pp \to W' \to WH) < 7.1$ fb are also plotted.

vicinity of $c_\phi \sim 0.73$ and $s_{2\beta} \sim 0.9$, $\sigma(W') \times \mathrm{BR}(W' \to WH) \sim 3$ fb which is below the current experimental limit of $\sigma(W') \times \mathrm{BR}(W' \to WH) < 7.1$ fb [4].

The cross section of $\sigma(W') \times \mathrm{BR}(W' \to e\nu)$ is shown in Fig. 4(c), which satisfies the current experimental upper limit $\sigma(pp \to W' \to e\nu/\mu\nu) \leq 0.7$ fb in the whole parameter space. The current bound on the tb mode demands $c_\phi < 0.91$; see Fig. 4(d).

In Fig. 5 we present the cross section $\sigma(W') \times \mathrm{BR}(W' \to XY)$ as a function of c_ϕ, where X and Y denote the SM particles in the W' decay. To see the maximally allowed region of c_ϕ, we consider the PDF uncertainties of the production cross section of W' and choose $s_{2\beta} = 1$. The outer dashed-curves represent the PDF uncertainties. The green shaded region represents the parameter space compatible with the WZ excess. The yellow shaded region is required for $M_{W'} \simeq M_{Z'}$. The current experimental limits of $\sigma(pp \to W' \to jj) < 102$ fb and $\sigma(pp \to W' \to WH) < 7.1$ fb are also plotted. The parameter space of $0.68 < c_\phi < 0.81$ can explain WZ excess and the current experimental upper limits of WH and jj. However, it predicts 2.47 TeV $< M_{Z'} < 2.94$ TeV which is in contradiction with the WW excess around 2 TeV. If further experiments confirm that the WW excess is owing to a fluctuation of the SM backgrounds, then the W' in the left-right model could explain the WZ excess.

2. The Z' constraints

The coupling of Z' to the SM fermions is very sensitive to the mixing angle $\phi = \arctan(g_X/g_2)$. In the limit of $x \gg 1$, $g_{L/R}^{Z'\bar{f}f} \sim 1/s_\phi c_\phi$. The couplings tend to be nonperturbative in the region of $c_\phi \sim 0$ or $c_\phi \sim 1$, yielding a large decay width of Z'; see the Fig. 6(a). We demand $\Gamma(Z') \leq 0.1 M_{Z'}$ in this work, which requires $0.23 \leq c_\phi \leq 0.96$. Figure 6(b) displays the branching ratios of all the decay modes of Z'. The jj mode includes all the light quark flavors (u, d, c, s, b), the $\ell\ell$ mode sums over the charged leptons while the $\nu\nu$ mode sums over all the three neutrino final states. We single out the top-quark pair mode (tt) to compare to the latest experimental data. The WW and ZH modes are much smaller than other modes; see the red-solid curve.

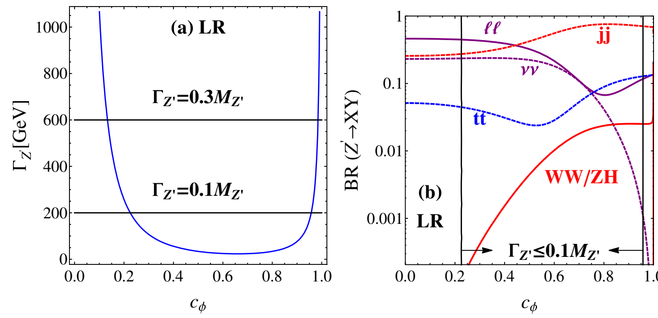

FIG. 6 (color online). The total width (a) and the branching ratios of all the decay modes (b) of Z' as a function of c_ϕ. The jj mode includes all the light quark flavors (u, d, c, s, b), the tt mode denotes the top-quark pair final state, the $\ell\ell$ mode sums over the charged leptons while the $\nu\nu$ mode sums over all the three neutrino final states.

In Fig. 7 we present the cross section $\sigma(Z') \times \mathrm{BR}(Z' \to XY)$ as a function of c_ϕ, where X and Y denote the SM particles in the Z' decay. The curves show the theoretical predictions while the shaded bands along each curve represent the parameter space compatible with current experimental data. The current bound on $\sigma(Z') \times \mathrm{BR}(Z' \to t\bar{t})$ mode demands $0.16 \leq c_\phi \leq 0.88$; see the blue-dotted curve with the tt label. The di-jet (jj) constraint is slightly weaker than the tt constraint. The shaded band along the WW/ZH curve (red-solid) represents the required c_ϕ to explain the WW excess. However, all the parameter space of interest to us is excluded by the leptonic decay mode, which imposes much tighter constraint of $\sigma(Z') \times \mathrm{BR}(Z' \to e^+e^-) \leq 0.2$ fb [23,24]. As shown in

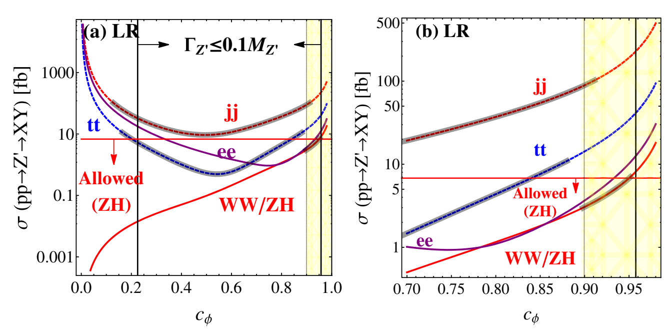

FIG. 7 (color online). The contours of the cross section $\sigma(Z') \times \mathrm{BR}(Z' \to XY)$, where X and Y denote the SM particles in the Z' decay as a function of c_ϕ. The shaded bands along each curve represent the region compatible with the current experimental data. The yellow shaded region is required for $M_{W'} \simeq M_{Z'}$.

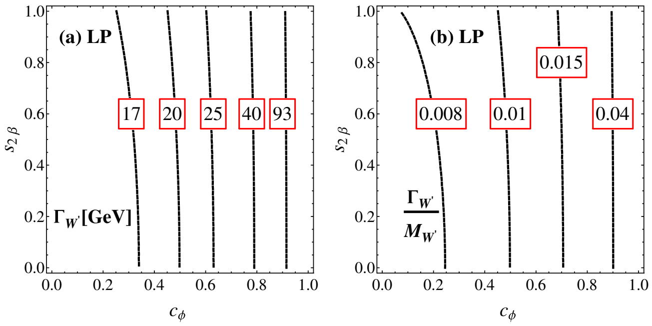

FIG. 8 (color online). The total width $\Gamma_{W'}$ (a) and $\Gamma_{W'}/M_{W'}$ (b) in the plane of c_ϕ and $s_{2\beta}$ in the leptophobic doublet model.

Fig. 7(b), $\sigma(Z') \times \mathrm{BR}(Z' \to e^+e^-) \sim 1$ fb for a 2 TeV Z' boson; see the purple curve. We thus conclude that, if the WW excess is induced by the Z' boson in the left-right model, one needs to extend the model to suppress the leptonic decays of the Z' boson.

B. Leptophobic doublet model

1. The W' constraints

The leptophobic doublet model is similar to the left-right model but the leptonic doublet is gauged only under $SU(1)_1$; see Table I. Figure 8 displays the contour of the total width $\Gamma_{W'}$ and $\Gamma_{W'}/M_{W'}$ in the plane of c_ϕ and $s_{2\beta}$. It shows the NWA is also a good approximation to describe the production and decay of W'.

Figure 9(a) displays the contour of the cross section of $\sigma(W') \times \mathrm{BR}(W' \to WZ)$ in the plane of c_ϕ and $s_{2\beta}$. The yellow bands represent the degenerated region of $M_{W'}$ and $M_{Z'}$. In order to produce $\sigma(WZ) \sim 4$–8 fb and $\sigma(W') \times \mathrm{BR}(W' \to jj) \leq 102$ fb [20], one needs $0.73 < c_\phi < 0.75$ and $s_{2\beta} \gtrsim 0.9$. However, the Z' mass in those parameter space is much larger than the W' mass, e.g., 2.67 TeV $\leq M_{Z'} < 2.74$ TeV for $M_{W'} = 2$ TeV. As analogous to the left-right model, the leptophobic model can explain the WZ excess if the WW excess is a result of the fluctuation of SM backgrounds.

Figure 9(b–d) shows the cross sections of $\sigma(W') \times \mathrm{BR}(W' \to WH/e\nu/tb)$, respectively. In the region of $0.73 < c_\phi < 0.75$, all of those three modes satisfy the current experimental upper limits.

Similar to the left-right model, we choose $s_{2\beta} = 1$ and plot the cross section of $pp \to W' \to WZ/WH$ (red curves) and $pp \to W' \to jj$ (blue curves) as a function of c_ϕ in Fig. 10. The outer dashed-curves represent the PDF uncertainties. The green shaded region represents the parameter space compatible with the WZ excess. The yellow shaded region is required for $M_{W'} \simeq M_{Z'}$. The current experimental limits of $\sigma(pp \to W' \to jj) < 102$ fb and $\sigma(pp \to W' \to WH) < 7.1$ fb are also plotted. To explain the excess of the WZ and satisfy WH limit, it requires $0.68 < c_\phi < 0.88$, while the dijet experimental limit requires $c_\phi < 0.81$. Thus, we conclude that the leptophobic model could explain the WZ excess in the region $0.68 < c_\phi < 0.81$ with $s_{2\beta} \sim 1$. However, it predicts a heavier Z' as 2.47 TeV $\leq M_{Z'} < 2.94$ TeV for $M_{W'} = 2$ TeV, which contradicts the WW excess around 2 TeV. Bearing in mind that the $2.6\sigma WW$ excess might be owing to the fluctuation of the SM backgrounds, we await the

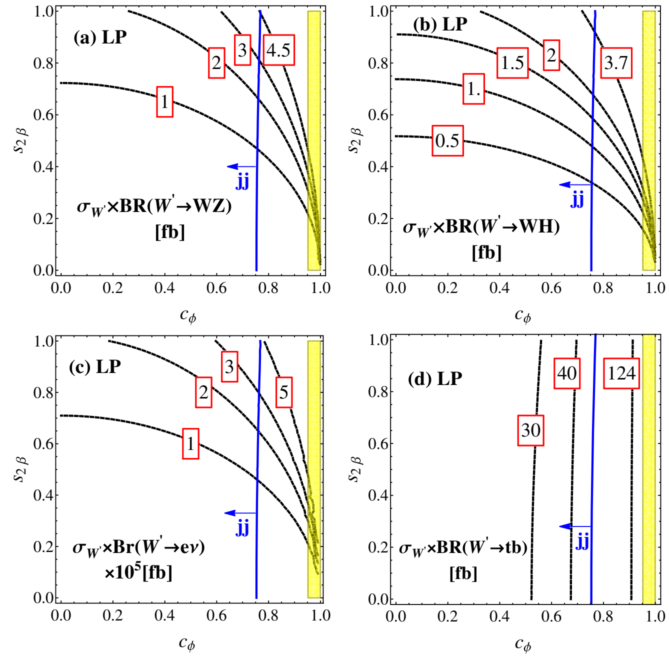

FIG. 9 (color online). The contours of the cross section (a) $\sigma(W') \times \mathrm{BR}(W' \to WZ)$, (b) $\sigma(W') \times \mathrm{BR}(W' \to WH)$, (c) $\sigma(W') \times \mathrm{BR}(W' \to e\nu)$, and (d) $\sigma(W') \times \mathrm{BR}(W' \to tb)$ in the plane of c_ϕ and $s_{2\beta}$. The vertical line (jj) denotes the constraint from the dijet measurements. The yellow band represents the degenerated mass region of W' and Z'.

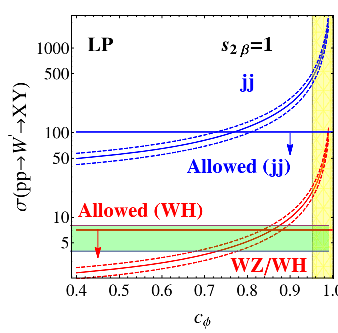

FIG. 10 (color online). The cross section of $pp \to W' \to WZ/WH$ (red curves) and $pp \to W' \to jj$ (blue curves) as a function of c_ϕ with $s_{2\beta} = 1$. The dashed curves represent the PDF uncertainties. The green shaded region represents the parameter space compatible with the WZ excess. The yellow shaded region is required for $M_{W'} \simeq M_{Z'}$. The current experimental limits of $\sigma(pp \to W' \to jj) < 102$ fb and $\sigma(pp \to W' \to WH) < 7.1$ fb are also plotted.

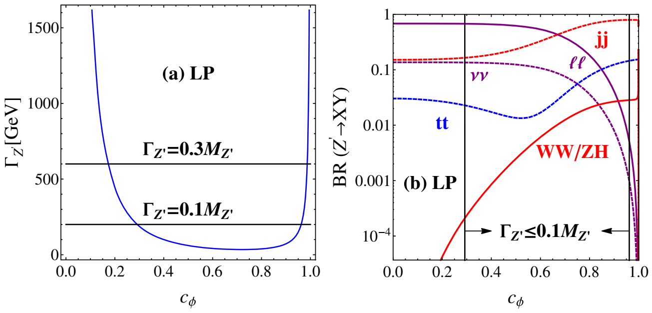

FIG. 11 (color online). The total width (a) and the branching ratios of all the decay modes (b) of Z' as a function of c_ϕ in leptophobic model.

forthcoming LHC Run-2 data to make an affirmative conclusion.

2. *The Z' constraints*

Although the couplings of W' to the SM leptons are highly suppressed in the leptophobic model, the couplings of Z' to the SM leptons are not. For a small c_ϕ (large g_X), the $U(1)_X$ component in the Z' gives rise to a large coupling to the SM leptons. That yields a large decay width of Z' in the vicinity of $c_\phi \sim 0$. We also require $\Gamma(Z') \leq 0.1 M_{Z'}$ which leads to $0.29 \leq c_\phi \leq 0.96$; see Fig. 11(a). Figure 11(b) displays the branching ratios of the Z' decay. It shows the branching ratios of $Z' \to \nu\nu$ and $Z' \to \ell\ell$ are suppressed for a large c_ϕ while the jj and $t\bar{t}$ decay modes tend to be dominate. Such a behavior can be understood from the fact that heavy gauge bosons are predominately coupled to the SM quarks. The WW and ZH modes are also much smaller than other modes; see the red-solid curve.

In Fig. 12 we present $\sigma(Z') \times \mathrm{BR}(Z' \to XY)$ as a function of c_ϕ where X and Y denote the SM particles in the Z' decay. The curves show the theoretical predictions while the shaded bands are allowed by current experimental data. The current bound on $\sigma(Z') \times \mathrm{BR}(Z' \to t\bar{t})$ mode demands $0.13 \leq c_\phi \leq 0.88$; see the blue-dotted curve with the tt label. The dijet (jj) constraint is slighter weaker than the tt constraint. The shaded band along the WW/ZH curve (red-solid) represents the required c_ϕ to explain the WW excess, i.e., $0.89 < c_\phi < 0.95$. However, all the parameter space of interest to us is excluded by the leptonic decay mode, which imposes much tighter constraint of $\sigma(Z') \times \mathrm{BR}(Z' \to e^+e^-) \leq 0.2$ fb [23,24]; see the purple-solid curve. Figure 12(b) shows the details in the vicinity of $c_\phi \sim 0.9$. The cross section of $\sigma(Z') \times \mathrm{BR}(Z' \to e^+e^-) \sim 1$ fb, which is much larger than the current constraint. Therefore, it is difficult to explain the WW excess in the leptophobic model unless one can sizeably reduce the leptonic decay branching ratio of Z'.

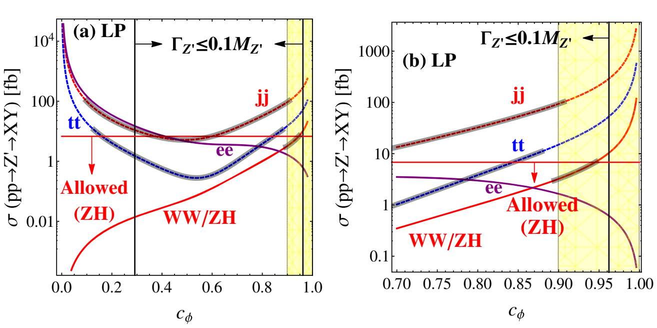

FIG. 12 (color online). The contours of the cross section $\sigma(Z') \times \mathrm{BR}(Z' \to XY)$, where X and Y denote the SM particles in the Z' decay as a function of c_ϕ in the leptophobic model.

C. Hadrophobic doublet model

1. *The W' constraints*

In the hadrophobic doublet model the right-handed leptons form a doublet gauged under the $SU(2)_2$; see Table I for detailed quantum number assignments. The W' and Z' arise from the symmetry breaking of $SU(2)_2 \times U(1)_X \to U(1)_Y$ and therefore are coupled predominately to the SM leptons.

Figure 13 displays the contour of the total width $\Gamma_{W'}$ (a) and the ratio $\Gamma_{W'}/M_{W'}$ (b) in the plane of c_ϕ and $s_{2\beta}$. In the most of the parameter space, the W' width is around 1 GeV for a 2 TeV W'. Therefore, the NWA is a good approximation to describe the production and decay of W' in the hadrophobic model.

As the gauge couplings of W' to the SM quarks are highly suppressed, the production cross section of W' in the hadrophobic model is much smaller than those in the left-right and leptophobic models. Figure 14 displays the contour of the cross section of $\sigma(W') \times \mathrm{BR}(W' \to WZ/WH/e\nu/tb)$ in the plane of c_ϕ and $s_{2\beta}$. The yellow shaded region is required for $M_{W'} \simeq M_{Z'}$. The cross sections of $pp \to W' \to WZ$ and $pp \to W' \to WH$ are around 10^{-4} fb. Since the W' boson couples to the SM leptons/quarks through the mixing of W-W', the branching ratio of W' decaying into lepton/quark final states are highly suppressed, yielding $\sigma(W') \times \mathrm{BR}(W' \to e\nu/tb/jj) \sim 10^{-9}$ fb. It is clear that, in all the parameter

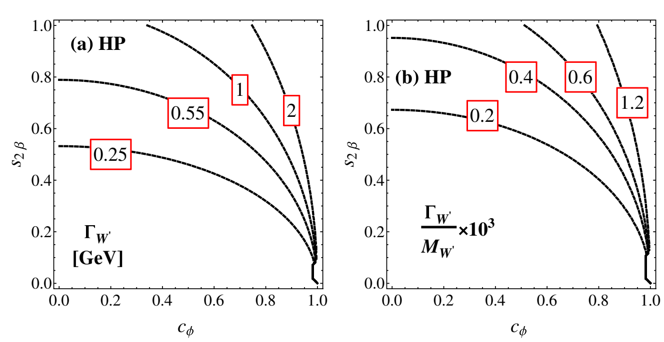

FIG. 13 (color online). The total width $\Gamma_{W'}$ (a) and $\Gamma_{W'}/M_{W'}$ (b) in the plane of c_ϕ and $s_{2\beta}$ in the hadrophobic doublet model.

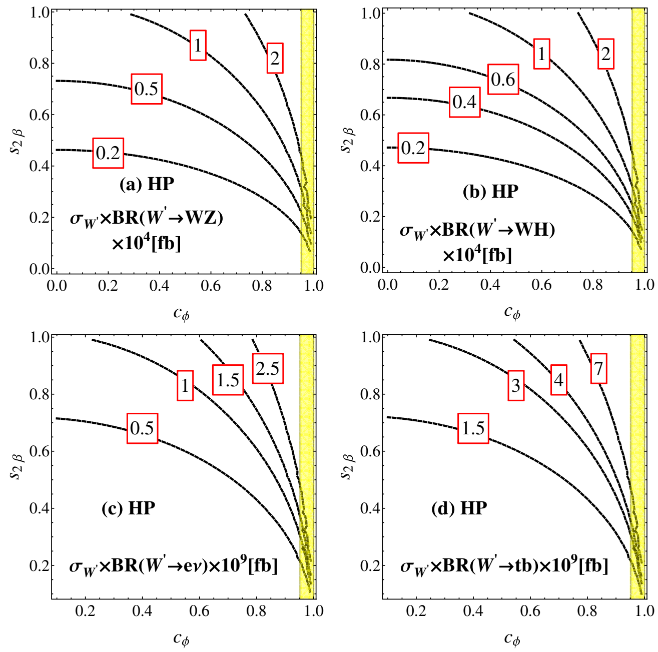

FIG. 14 (color online). The contours of the cross section (a) $\sigma(W') \times \mathrm{BR}(W' \to WZ)$, (b) $\sigma(W') \times \mathrm{BR}(W' \to WH)$, (c) $\sigma(W') \times \mathrm{BR}(W' \to e\nu)$ and (d) $\sigma(W') \times \mathrm{BR}(W' \to tb)$ in the plane of c_ϕ and $s_{2\beta}$ in the hadrophobic doublet model. All the cross sections are in the unit of fb. The yellow shaded region is required for $M_{W'} \simeq M_{Z'}$.

space, the cross section of the WZ mode is much smaller than 1 fb such that it cannot explain the WZ excess.

2. The Z' constraints

Now we consider the phenomenology of the Z' boson in the hadrophobic doublet model. We require $\Gamma(Z') \le 0.1 M_{Z'}$, which leads to $0.34 \le c_\phi \le 0.99$; see Fig. 15(a). Figure 15(b) displays the decay branching ratios of Z'. We note that the branching ratio of $Z' \to jj$ and $Z' \to t\bar{t}$ is suppressed for a large c_ϕ as one can see from Eq. (14).

In Fig. 16 we present the cross section $\sigma(Z') \times \mathrm{BR}(Z' \to XY)$ as a function of c_ϕ. The curves show the theoretical

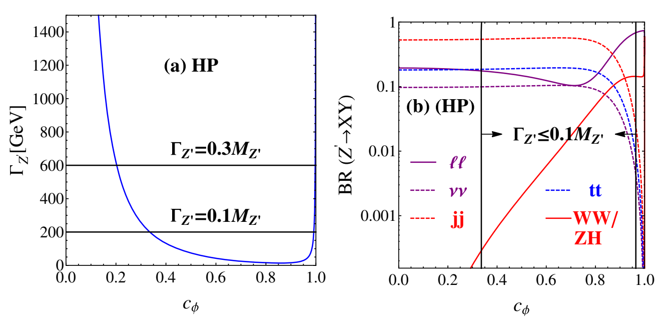

FIG. 15 (color online). The total width $\Gamma_{Z'}$ (a) and the branching ratios of the Z' decay (b) as a function of c_ϕ in hadrophobic model.

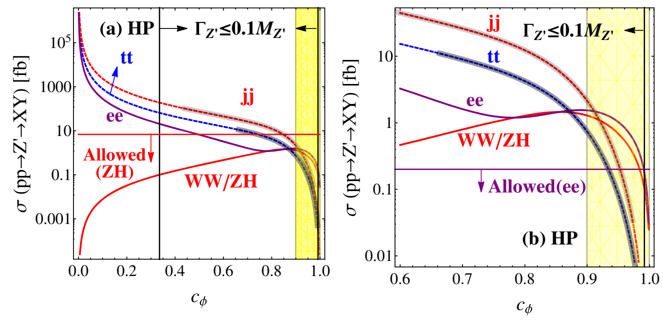

FIG. 16 (color online). The contours of the cross section of $\sigma(Z') \times \mathrm{BR}(Z' \to XY)$, where X and Y denote the SM particles in the Z' decay as a function of c_ϕ in the hadrophobic model. The shaded bands are corresponding to the allowed regions by the current experimental data. The yellow shaded region is required for $M_{W'} \simeq M_{Z'}$.

predictions while the shaded band along each curve is allowed by current experimental data. The yellow shaded region is required for $M_{W'} \simeq M_{Z'}$. The current bound on $\sigma(Z') \times \mathrm{BR}(Z' \to t\bar{t})$ mode demands $0.66 \le c_\phi \le 1$; see the blue-dashed curve with the tt label. The dijet constraint is slightly weaker than the tt constraint. There is no parameter space to explain the WW excess. Furthermore, the cross section $\sigma(Z') \times \mathrm{BR}(Z' \to ee)$ is above the current experimental constraint; see Fig. 16(b) for details. Thus, we conclude that it cannot explain the WW excess in the hadrophobic model.

D. Fermiophobic doublet model

1. The W' constraints

Finally, we examine the fermiophobic doublet model in which both the SM quark and lepton doublets are gauged only under $SU(1)_1$; see Table I. The gauge couplings of W' to SM fermions are suppressed due to the fact that the SM fermions are not gauged under gauge group $SU(2)_2$. The W' width in the fermiophobic model is less than the W' width in the leptophobic and hadrophobic models. Figure 17 displays the contour of the total width $\Gamma_{W'}$

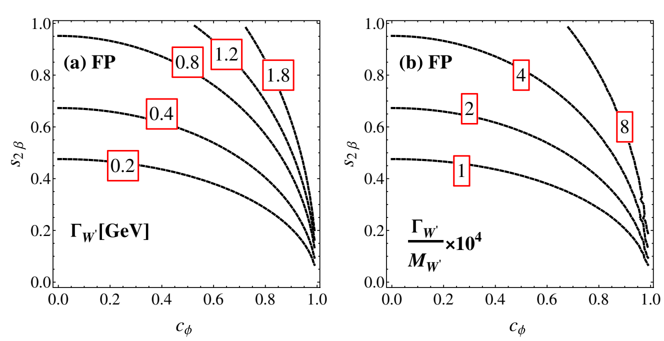

FIG. 17 (color online). The total width $\Gamma_{W'}$ (a) and $\Gamma_{W'}/M_{W'}$ (b) in the plane of c_ϕ and $s_{2\beta}$ in the fermiophobic doublet model.

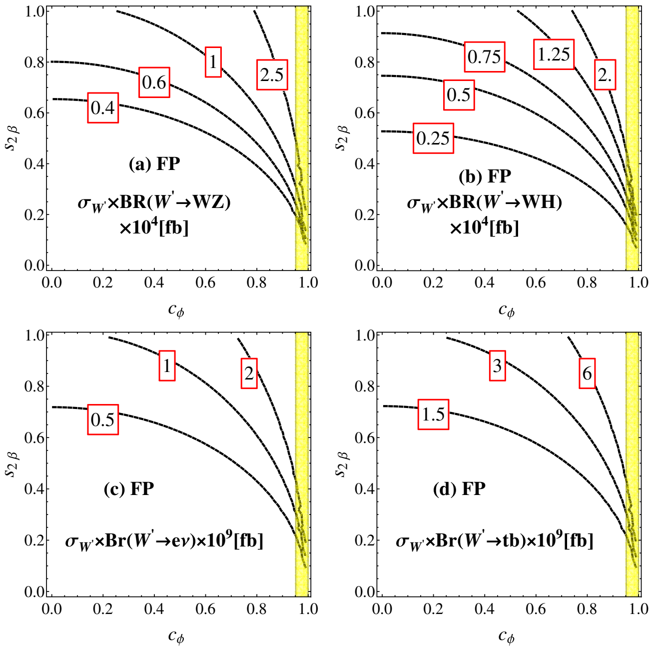

FIG. 18 (color online). The contours of the cross section (a) $\sigma(W')\times \mathrm{BR}(W'\to WZ)$, (b) $\sigma(W')\times \mathrm{BR}(W'\to WH)$, (c) $\sigma(W')\times \mathrm{BR}(W'\to e\nu)$ and (d) $\sigma(W')\times \mathrm{BR}(W'\to tb)$ in the plane of c_ϕ and $s_{2\beta}$ in the fermiophobic doublet model. The yellow shaded region is required for $M_{W'}\simeq M_{Z'}$.

and $\Gamma_{W'}/M_{W'}$ in the plane of c_ϕ and $s_{2\beta}$. Again, the NWA is a good approximation in the fermiophobic doublet model.

The production cross section of W' in the model is much smaller than the cross section in the left-right and leptophobic models. It is, however, comparable to the hadrophobic model. Figure 18 displays the contour of the cross section of $\sigma(W')\times \mathrm{BR}(W'\to WZ/WH/e\nu/tb)$ in the plane of c_ϕ and $s_{2\beta}$. The yellow shaded region is required for $M_{W'}\simeq M_{Z'}$. Owing to the suppress of the production rate, the typical value of cross section in WZ and WH modes are around 10^{-4} fb. The branching ratios of W' decay to lepton/quark final states are suppressed dramatically due to the W-W' mixing and leads to $\sigma(W')\times \mathrm{BR}(W'\to e\nu/tb/jj)\sim 10^{-9}$ fb. It is clear that the cross section at the all parameter space is much smaller than 1 fb such that it cannot explain the WZ excess.

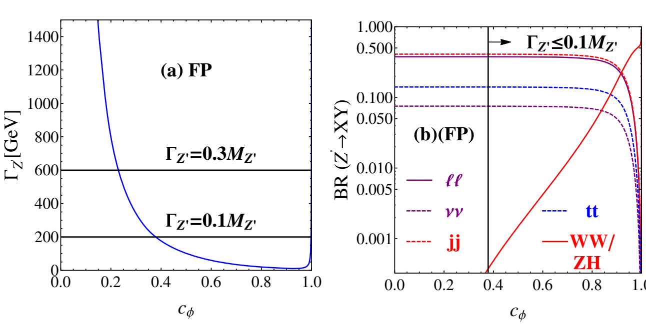

FIG. 19 (color online). The total width (a) and the branching ratios of Z' decays (b) as a function of c_ϕ in fermiophobic model.

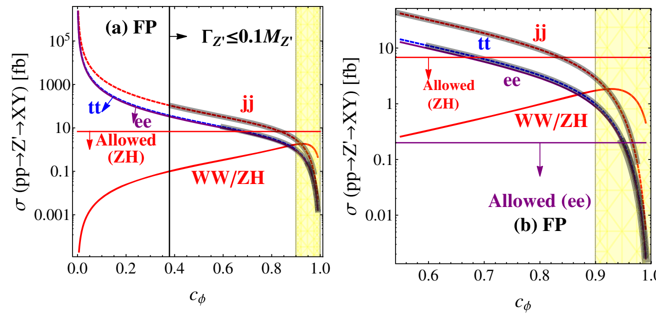

FIG. 20 (color online). The cross section contours of $\sigma(Z')\times \mathrm{BR}(Z'\to XY)$, where X and Y denote the SM particles in the Z' decay as a function of c_ϕ in the fermiophobic model. The yellow shaded region is required for $M_{W'}\simeq M_{Z'}$.

2. The Z' constraints

In the fermiophobic doublet model, the Z' couples to the SM fermions via the $U(1)_X$ component and the coupling strength is large in the region of $c_\phi\sim 0$ where $g_X\gg g_2$. We require $\Gamma(Z')\leq 0.1M_{Z'}$, which leads to $c_\phi\geq 0.38$; see Fig. 19(a). Figure 19(b) displays the branching ratios of all the decay modes of Z'. We note that the branching ratio of $Z'\to WW$ and $Z'\to ZH$ is highly enhanced for a large c_ϕ, e.g., $\mathrm{BR}(Z'\to WW/ZH)>0.1$ when $c_\phi>0.85$, which is different from other BP-I models. It is owing to the fact that the decay rate of W' to SM fermions is highly suppressed when $c_\phi\to 1$ in this model.

In Fig. 20 we present the cross section $\sigma(Z')\times \mathrm{BR}(Z'\to XY)$, where X and Y denote the SM particles in the Z' decay, as a function of c_ϕ. The curves show the theoretical predictions while the shaded bands are allowed by current experimental data. The yellow shaded region is required for $M_{W'}\simeq M_{Z'}$. The current bound on $\sigma(Z')\times \mathrm{BR}(Z'\to t\bar{t})$ mode, denoted as tt in the figure, demands $0.6\leq c_\phi\leq 1$. The dijet constraint is slightly weaker than the tt constraint. The whole parameter space satisfies the current bound on $\sigma(Z')\times \mathrm{BR}(Z'\to ZH)$, but cannot explain the excess of WW. Again, the leptonic decay mode imposes much tighter constraint as $\sigma(Z')\times \mathrm{BR}(Z'\to e^+e^-)\leq 0.2$ fb by the current measurements [23,24], which requires $c_\phi>0.95$. Thus we conclude that the fermiophobic doublet model cannot explain the WW excess.

V. $G(221)$ MODELS: BREAKING PATTERN II

In the BP-II, $U(1)_X$ is identified as the $U(1)_Y$ of the SM. The first stage of symmetry breaking $SU(2)_1\times SU(2)_2\to SU(2)_L$ occurs at the TeV scale, which is owing to a scalar bi-doublet $\Phi\sim(2,\bar{2},0)$ with only one VEV u. The subsequent breaking of $SU(2)_L\otimes U(1)_Y\to U(1)_{\mathrm{em}}$ at the electroweak scale is generated by a Higgs doublet $H \sim (2, 1, 1/2)$ with a VEV v. The explicit forms of the bidoublet and doublet as well as their vacuum expectation values are given as follows:

$$\Phi = \begin{pmatrix} \phi^0 & \sqrt{2}\phi^+ \\ \sqrt{2}\phi^- & \phi^0 \end{pmatrix}, \qquad \langle\Phi\rangle = \frac{1}{2}\begin{pmatrix} u & 0 \\ 0 & u \end{pmatrix},$$
$$H = \begin{pmatrix} h^+ \\ h^0 \end{pmatrix}, \qquad \langle H\rangle = \frac{1}{\sqrt{2}}\begin{pmatrix} 0 \\ v \end{pmatrix}. \tag{15}$$

In the BP-II, the couplings of the three gauge groups are

$$g_1 = \frac{e}{s_W c_\phi}, \qquad g_2 = \frac{e}{s_W s_\phi}, \qquad g_X = \frac{e}{c_W}, \tag{16}$$

where $\phi = \arctan(g_2/g_1)$ is the mixing angle. After the symmetry breaking both W' and Z' bosons obtain their masses and are degenerated at the tree level,

$$M^2_{W'^\pm} = M^2_{Z'} = \frac{e^2 v^2}{4 s_W^2 s_\phi^2 c_\phi^2}(x + s_\phi^4). \tag{17}$$

The gauge couplings of W' and Z' to the SM Higgs boson and gauge bosons are generated after the second stage of the symmetry breaking, which are given as follows,

$$HW_\nu W'_\rho\colon \frac{1}{2}\frac{e^2 s_\phi}{s_W^2 c_\phi} v g_{\nu\rho}\left[1 + \frac{s_\phi^2(c_\phi^2 - s_\phi^2)}{x}\right],$$
$$HZ_\nu Z'_\rho\colon \frac{1}{2}\frac{e^2 s_\phi}{c_W s_W^2 c_\phi} v g_{\nu\rho}\left[1 - \frac{s_\phi^2(s_\phi^2 c_W^2 - c_\phi^2)}{x c_W^2}\right],$$
$$W^+_\mu W'^-_\nu Z_\rho\colon \frac{e c_\phi s_\phi^3}{x c_W s_W},$$
$$W^+_\mu W^-_\nu Z'_\rho\colon \frac{e c_\phi s_\phi^3}{x s_W}. \tag{18}$$

In BP-II the bosonic decays of W'/Z' in the limit of $x \gg 1$ and $M_{W'} \gg m_{W/Z/H}$ are correlated as follows

$$\frac{\mathrm{BR}(W' \to WZ)}{\mathrm{BR}(W' \to WH)} \sim 1, \qquad \frac{\mathrm{BR}(Z' \to WW)}{\mathrm{BR}(Z' \to ZH)} \sim 1. \tag{19}$$

The couplings of the W' bosons to the SM fermions in the BP-II are

$$g_L^{W'\bar{f}f'} = \frac{e s_\phi}{\sqrt{2} s_W c_\phi}\gamma^\mu\left(1 + \frac{s_\phi^2 c_\phi^2}{x}\right), \qquad g_R^{W'\bar{f}f'} = 0,$$
$$g_L^{W'\bar{F}F'} = -\frac{e c_\phi}{\sqrt{2} s_W s_\phi}\gamma^\mu\left(1 - \frac{s_\phi^4}{x}\right), \qquad g_R^{W'\bar{F}F'} = 0. \tag{20}$$

while those of the Z' boson are

$$g_L^{Z'\bar{f}f} = \frac{e}{s_W}\gamma^\mu\left[\frac{s_\phi}{c_\phi}T_3^1\left(1 + \frac{s_\phi^2 c_\phi^2}{x c_W^2}\right) - \frac{s_\phi}{c_\phi}\frac{s_\phi^2 c_\phi^2}{x c_W^2}s_W^2 Q\right],$$
$$g_R^{Z'\bar{f}f} = -\frac{e}{s_W}\gamma^\mu\left(\frac{s_\phi}{c_\phi}\frac{s_\phi^2 c_\phi^2}{x c_W^2}s_W^2 Q\right),$$
$$g_L^{Z'\bar{F}F} = -\frac{e}{s_W}\gamma^\mu\left[\frac{c_\phi}{s_\phi}T_3^2\left(1 - \frac{s_\phi^4}{x c_W^2}\right) + \frac{c_\phi}{s_\phi}\frac{s_\phi^4}{x c_W^2}s_W^2 Q\right],$$
$$g_R^{Z'\bar{F}F} = -\frac{e}{s_W}\gamma^\mu\left(\frac{c_\phi}{s_\phi}\frac{s_\phi^4}{x c_W^2}s_W^2 Q\right), \tag{21}$$

where f represents the fermions are gauged under $SU(2)_1$ while F the fermions gauged under $SU(2)_2$.

Next we consider un-unified model and non-universal/top-flavor model, and discuss their implications in the production of W'/Z' and their decay modes of the $WZ/WW/WH/ZH$ pair at the LHC.

A. Un-unified model

1. The W' constraints

We begin with the un-unified model in which the left-handed quarks are gauged under $SU(2)_1$ while the lepton doublets gauged under $SU(2)_2$. Figure 21(a) shows the total width $\Gamma_{W'}$ as a function of c_ϕ. The W' couples to the SM quarks and leptons strongly in the region of $c_\phi \sim 0$ and

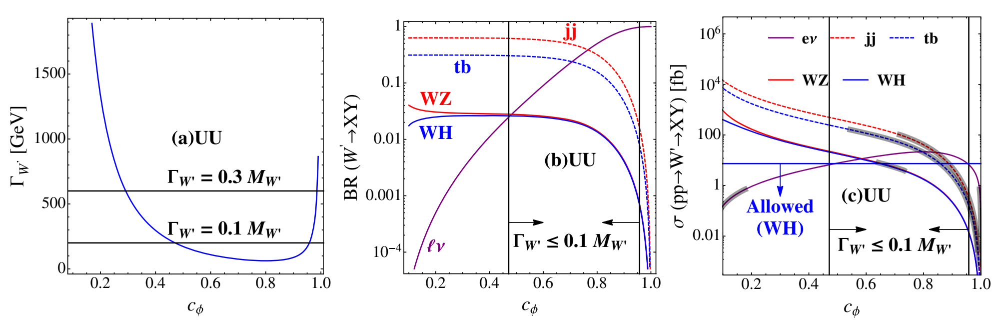

FIG. 21 (color online). (a) The total width $\Gamma_{W'}$ as a function of c_ϕ in the un-unified (UU) model of BP-II. (b) The decay branching ratio $BR(W' \to XY)$ as a function of c_ϕ. (c) The cross section $\sigma(pp \to W' \to XY)$ as a function of c_ϕ at the LHC Run-1. The shaded band of each curve satisfies the current experiment data.

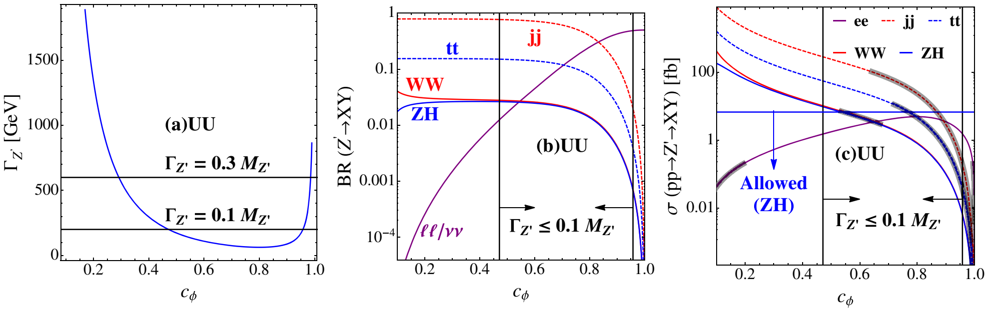

FIG. 22 (color online). (a) The total width $\Gamma_{Z'}$ as a function of c_ϕ in the un-unified (UU) model of BP-II. (b) The decay branching ratio $\mathrm{BR}(Z' \to XY)$ as a function of c_ϕ in the un-unified (UU) model of BP-II. (c) The cross section $\sigma(pp \to Z' \to XY)$ at LHC Run-1 as a function of c_ϕ in the un-unified (UU) model of BP-II. The shaded band of each curve satisfies the current experiment.

$c_\phi \sim 1$, respectively. That yields a wide width of W'. In order to validate the NWA, we demand $\Gamma_{W'} \leq 0.1 M_{W'}$ which is presented by the black horizontal line. It requires $0.47 \leq c_\phi \leq 0.96$.

The branching ratios of W' are plotted in Fig. 21(b). For a large c_ϕ, the branching ratio of $W' \to jj/tb$ are suppressed while the branching ratio of $W' \to l\nu$ is enhanced. Such a behavior can be understood from the gauge coupling of W' to the SM fermions; see Eq. (20). The coupling of W' to the SM quarks is proportional to $\tan\phi$, while for the leptons, the gauge coupling is proportional to $\cot\phi$. The branching ratios of $W' \to WZ/WH$ can reach ~0.01 for most of the parameter space in the model. Figure 21(c) shows the cross sections of $\sigma(W') \times \mathrm{BR}(W' \to XY)$. The shaded bands are consistent with current experimental data. In order to explain the WZ excess, one needs $0.64 < c_\phi < 0.73$. However, the jj mode requires $c_\phi > 0.72$. There is a tension between the WZ mode and the jj mode. The negative searching result of the WH mode demands $c_\phi > 0.65$. It is possible to satisfy the WZ, jj and WH modes within 2σ confidential level.

We also plot the cross section of the leptonic decay in Fig. 21(c). Unfortunately, the cross section of $\sigma(W') \times \mathrm{BR}(W' \to e\nu)$ in the region of $c_\phi \sim 0.4$–0.7 is far beyond the current experimental limit. In order to explain the WZ excess in the un-unified model, one has to extend the model to reduce the leptonic decay mode.

2. The Z' constraints

Figure 22 shows the total width $\Gamma_{Z'}$ (a) and decay branching ratios of Z' (b) as a function of c_ϕ. We also demand the narrow width constraint $\Gamma_{Z'} \leq 0.1 M_{Z'}$, which also requires $0.47 \leq c_\phi \leq 0.96$. In analogue with W', the branching ratios of $Z' \to jj$ and $Z' \to t\bar{t}$ are suppressed, while the branching ratio of $Z' \to ll/\nu\nu$ are enhanced in the region of large c_ϕ. Note that the branching ratios of $W' \to WZ/WH$ are independent on the variable c_ϕ in the range $0.3 \leq c_\phi \leq 0.7$, which is about 0.03. Figure 21(c) shows the cross section of various decay modes of Z'. We observe a tension between the WW mode and the jj mode. Again, the leptonic decay mode imposes much tighter constraint as $\sigma(Z') \times \mathrm{BR}(Z' \to e^+e^-) \leq 0.2$ fb by the current measurements [23,24], which requires $c_\phi < 0.19$. Similar to the case of the W' boson, it is also possible to explain the WW excess if there exists some mechanism to decrease the leptonic decay mode of the Z' boson.

B. Nonuniversal model

1. The W' constraints

The nonuniversal model is often named as the top-flavor model. In the model, the left-handed fermions of the first two generations are gauged under $SU(2)_1$, while the left-handed fermions of the third generation are gauged under $SU(2)_2$; see Table I for the detail charge assignments. The W' couples strongly to the first two generation fermions in the region of $c_\phi \sim 0$ and to the third generation fermions in the region of $c_\phi \sim 1$. Figure 23(a) displays the decay width of W' versus c_ϕ. In order to validate the NWA, we demand $\Gamma_{W'} \leq 0.1 M_{W'}$ which is presented by the black-dashed horizontal line. It requires $0.45 \leq c_\phi \leq 0.95$. The branching ratios of the W' decays are also plotted in Fig. 23(b). Here we separate the first two generations of the SM fermions from the third generation. The $\ell\nu$ mode includes the first two generation of leptons ($e\nu$ and $\mu\nu$). For a large c_ϕ, the branching ratio of $W' \to \ell\nu$ and $W' \to jj$ are suppressed while the branching ratio of $W' \to \tau\nu$ and $W' \to tb$ are enhanced. It is owing to the fact that the gauge couplings of W' to the first two generation fermions are proportional to $\tan\phi$, while the gauge couplings to the third generation fermions are proportional to $\cot\phi$; see Eq. (20).

The branching ratios of $W' \to WZ/WH$ are about 0.01 for most of the parameter space. Figure 23(c) shows the cross sections of $\sigma(W') \times \mathrm{BR}(W' \to XY)$. The shaded bands are consistent with current experimental data. The WZ excess prefers $0.65 < c_\phi < 0.73$. However, there is a tension between the WZ mode and the jj mode as the jj mode requires $c_\phi > 0.72$. The negative searching result of

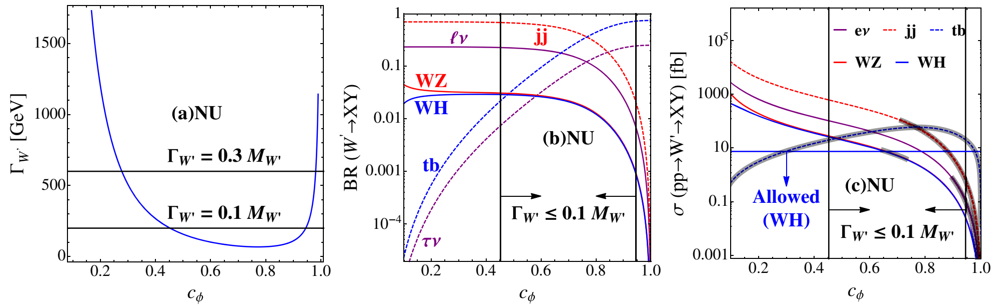

FIG. 23 (color online). (a) The total width $\Gamma_{W'}$ as a function of c_ϕ in the nonuniversal (NU) model of BP-II. (b) The decay branching ratio $\mathrm{BR}(W' \to XY)$ as a function of c_ϕ. (c) The cross section $\sigma(pp \to W' \to XY)$ versus c_ϕ at the LHC Run-1 in the NU model. The shaded band along each curve satisfies the current experimental data.

the WH mode demands $c_\phi > 0.66$. It is possible to satisfy the WZ, jj and WH modes within 2σ confidential level.

Unfortunately, the cross section of $\sigma(W') \times \mathrm{BR}(W' \to e\nu)$ in the region of $c_\phi \sim 0.4$–0.7 is far beyond the current experimental limit; see the purple solid curve in Fig. 23(c). In order to explain the WZ excess, one needs to introduce new ingredients into the nonuniversal model to reduce the leptonic decay modes of the W' boson.

2. The Z' constraints

Figure 24 shows the total width $\Gamma_{Z'}$ (a) and decay branching ratios of Z' (b) as a function of c_ϕ. We also demand the narrow width constraint $\Gamma_{Z'} \leq 0.1 M_{Z'}$ which also requires $0.45 \leq c_\phi \leq 0.95$. Here, the $\ell\ell$ mode sums over the electron (e) and muon (μ) while the $\nu\nu$ mode sums over the first two generation neutrinos.

We first notice that the jj mode dominates over the other modes in the entire parameter space of c_ϕ. The branching ratio of $Z' \to \ell\ell/\nu_\ell\nu_\ell$ is suppressed in the region of large c_ϕ. On the other hand, the branching ratios of $Z' \to tt$ and $Z' \to \tau\tau/\nu_\tau\nu_\tau$ are enhanced for a large c_ϕ. The branching ratios of $W' \to WZ/WH$ are not sensitive to c_ϕ in the range $0.3 \leq c_\phi \leq 0.7$, which is about 0.02. Figure 24(c) shows the cross section of various decay modes of Z'. We observe a tension between the WW mode and the jj mode. Again, the leptonic decay mode imposes much tighter constraint as $\sigma(Z') \times \mathrm{BR}(Z' \to e^+e^-) \leq 0.2$ fb by the current measurements [23,24], which requires $c_\phi > 0.89$. Again, it requires us to decrease the branching ratio of the leptonic decay mode in order to explain the WW excess in the nonuniversal model.

VI. $G(331)$ MODEL

Another simple non-Abelian extension of the SM gauge group is the so-called 331 model which exhibits a gauge structure of $SU(3)_C \otimes SU(3)_L \otimes U(1)_X$ [48–69]. The electroweak symmetry is broken spontaneously as follows,

$$SU(3)_L \times U(1)_X \to SU(2)_L \times U(1)_Y \to U(1)_{\mathrm{em}}, \tag{22}$$

by three scalar triplets ρ, η, and χ with vacuum expectation values as follows,

$$\langle\rho\rangle = \frac{1}{\sqrt{2}}\begin{pmatrix} 0 \\ v_\rho \\ 0 \end{pmatrix}, \qquad \langle\eta\rangle = \frac{1}{\sqrt{2}}\begin{pmatrix} v_\eta \\ 0 \\ 0 \end{pmatrix},$$

$$\langle\chi\rangle = \frac{1}{\sqrt{2}}\begin{pmatrix} 0 \\ 0 \\ v_\chi \end{pmatrix}. \tag{23}$$

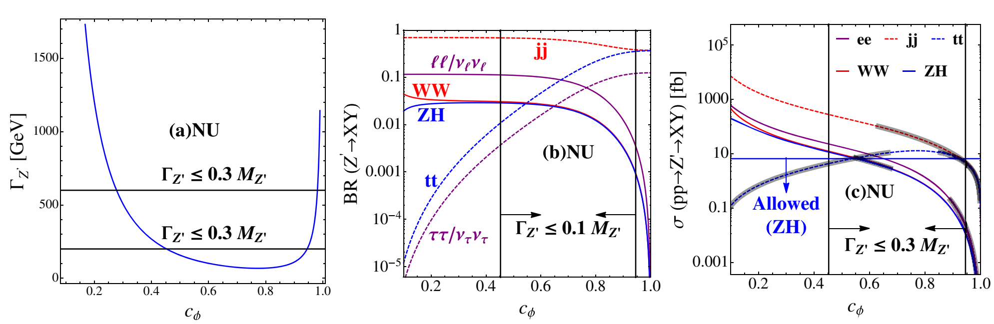

FIG. 24 (color online). (a) The total width $\Gamma_{Z'}$ versus c_ϕ in the nonuniversal (NU) model of BP-II. (b) The decay branching ratio $\mathrm{BR}(Z' \to XY)$ as a function of c_ϕ. (c) The cross section $\sigma(pp \to Z' \to XY)$ versus c_ϕ at the LHC Run-1. The shaded band along each curve satisfies the current experimental data.

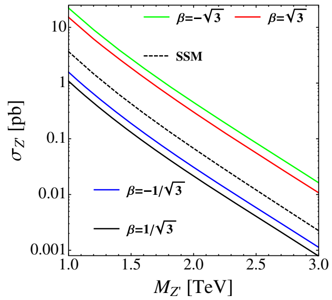

FIG. 25 (color online). The cross section of Z' production versus $M_{Z'}$ for different choices of β in the $G(331)$ model at the LHC Run-1. For comparison the production cross section of a sequential Z' boson is also plotted (black-dotted curve).

The χ triplet is responsible for the first step of symmetry breaking, while the ρ and η triplets are responsible for the second step of symmetry breaking.

The electric charge is defined as $Q = T_3 + Y = T_3 + \beta T_8 + X$ where T_i $(i = 1 \sim 8)$ are eight Gell-Mann Matrices and X is the quantum number associated with $U(1)_X$. The parameter β stands for the different definitions of the hypercharge Y or Q.

At the first step of spontaneously symmetry breaking at the TeV scale, three new gauge bosons Y, V, and Z' obtain their masses. The W and Z bosons are massive after the second step of symmetry breaking at the electroweak scale. Neglecting the small mixing of Z' and Z, the mass eigenstates of those gauge bosons can be written in terms of the $SU(3)_L$ and $U(1)_X$ gauge eigenstates W^i_μ $(i = 1 \sim 8)$ and X_μ as follows:

$$Y_\mu^{\pm Q_Y} = \frac{1}{\sqrt{2}}(W_\mu^4 \mp iW_\mu^5), \qquad V_\mu^{\pm Q_V} = \frac{1}{\sqrt{2}}(W_\mu^6 \mp iW_\mu^7),$$
$$Z'_\mu = -s_{331}W_\mu^8 + c_{331}X_\mu, \qquad W_\mu^{\pm} = \frac{1}{\sqrt{2}}(W_\mu^1 \mp iW_\mu^2),$$
$$Z_\mu = \frac{1}{\sqrt{g^2 + g_Y^2}}[gW_\mu^3 - g_Y(c_{331}W_\mu^8 + s_{331}X_\mu)], \tag{24}$$

where s_{331} and c_{331} are the sine and cosine of the 331 mixing angle, respectively, g_Y is the coupling strength of $U(1)_Y$. They can be written in terms of the $SU(3)_L$ and $U(1)_X$ coupling constants g and g_X as follows:

$$s_{331} = \frac{g}{\sqrt{g^2 + \beta^2 g_X^2}}, \qquad c_{331} = \frac{\beta g_X}{\sqrt{g^2 + \beta^2 g_X^2}},$$
$$g_Y = \frac{g g_X}{\sqrt{g^2 + \beta^2 g_X^2}}. \tag{25}$$

Owing to the gauge symmetry, the trilinear gauge couplings of $Y(V)WZ$ and $Z'ZZ$ are absent in the $G(331)$ model. It is difficult to explain the excesses observed by the ATLAS collaboration. The Z' can couple to the WW/ZH pair through the mixing with the Z boson. The mixing angle is [48],

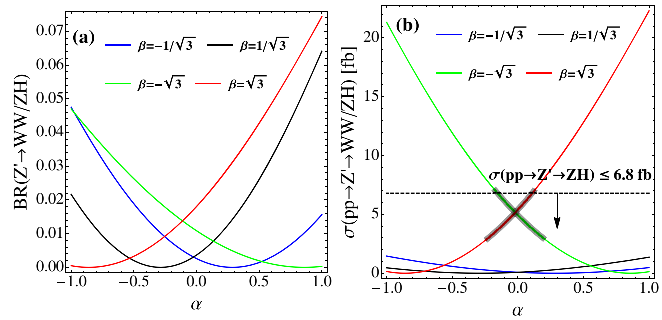

FIG. 26 (color online). (a) The branching ratio $\mathrm{BR}(Z' \to WW/ZH)$ as a function of α for different choices of β. (b) The cross section $\sigma(Z') \times \mathrm{BR}(Z' \to WW/ZH)$ as a function of α for different choices of β at the LHC Run-1. The shaded bands along the curves represent the parameter space that could explain the WW excess. The black-dashed horizontal line shows the upper limit of ZH.

$$\sin\theta_{ZZ'} = \frac{c_W^2}{3}\sqrt{f(\beta)}\left(3\beta\frac{s_W^2}{c_W^2} + \sqrt{3}\alpha\right)\frac{m_Z^2}{M_{Z'}^2}, \tag{26}$$

where

$$f(\beta) = \frac{1}{1-(1+\beta^2)s_W^2}, \qquad -1 < \alpha = \frac{v_-^2}{v_+^2} < 1, \tag{27}$$

with $v_+^2 = v_\eta^2 + v_\rho^2$ and $v_-^2 = v_\eta^2 - v_\rho^2$. Thus the branching ratios of $Z' \to WW$ and $Z' \to ZH$ are sensitive to α.

Figure 25 displays the cross section of the Z' production in the $G(331)$ model at the LO for various choices of β parameter. See Ref. [49] for the couplings of Z' to the SM fermions. For a 2 TeV resonance, the production cross sections $\sigma(Z')$ are 300 fb for $\beta = \sqrt{3}$, 454 fb for $\beta = -\sqrt{3}$, 21 fb for $\beta = +1/\sqrt{3}$ and 31 fb for $\beta = -1/\sqrt{3}$.

We first consider the decay mode of $Z' \to WW$ in the $G(331)$ model. Figure 26(a) displays the branching ratios of $\mathrm{BR}(Z' \to WW/ZH)$ for the four choices of β. The branching ratios are sensitive to the α parameter. Figure 26(b) displays the cross section of $\sigma(pp \to Z' \to WW/ZH)$ versus α. The shaded bands along the curves of $\beta = -\sqrt{3}$ and $\beta = \sqrt{3}$ denote the region that is compatible with the WW excess, where $-0.17 \le \alpha \le 0.19$ and $-0.23 \le \alpha \le 0.12$ for $\beta = -\sqrt{3}$ and $\beta = \sqrt{3}$, respectively. The current exclusion limit, $\sigma(pp \to Z' \to ZH) \le 6.8$ fb, is shown as the black-dashed horizontal curve.

Other decay modes of the Z' boson are also checked in this work. Figure 27 shows the cross section of Z' production with its subsequent decays into the SM quarks and leptons, i.e., (a) $\sigma(pp \to Z' \to t\bar{t})$, (b) $\sigma(pp \to Z' \to jj)$ and (c) $\sigma(pp \to Z' \to e^+e^-)$. The current experiment bounds are also plotted in the figure. The choices of

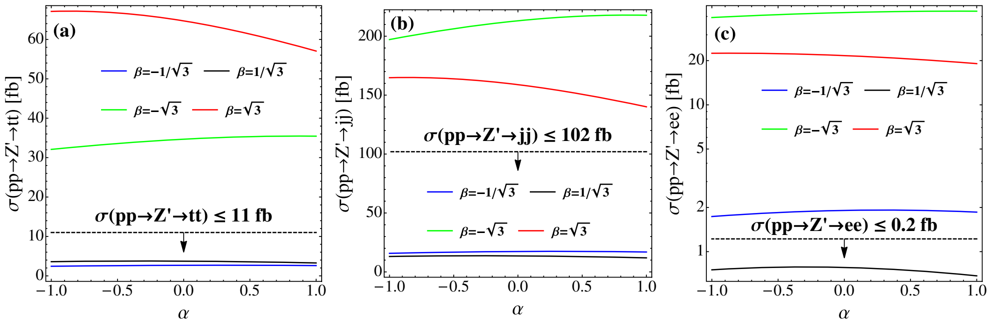

FIG. 27 (color online). The cross section of $\sigma(pp \to Z' \to t\bar{t})$ (a), $\sigma(pp \to Z' \to jj)$ (b) and $\sigma(pp \to Z' \to e\bar{e})$ (c) as a function of α in the $G(331)$ model. The current experimental limits are also displayed.

$\beta = \pm\sqrt{3}$ yield a large cross section which exceeds the current limits. Even though the choices of $\beta = \pm 1/\sqrt{3}$ are allowed, they cannot explain the 2.6σ excess in the WW channel.

VII. SUMMARY AND DISCUSSION

The excesses around 2 TeV in the diboson invariant mass distribution invoke excitement among theorists recently. We examine the possibility of explaining the resonances as extra gauge bosons. Two simple extensions of the SM gauge symmetry are explored. One is named as the $G(221)$ model with a gauge structure of $SU(2)_1 \times SU(2)_2 \times U(1)_X$, the other is called $G(331)$ model with $SU(3)_C \times SU(3)_L \times U(1)_X$ symmetry. Extra gauge bosons emerge after the symmetry is broken down to the SM gauge symmetry at the TeV scale in the breaking pattern (BP) listed as follows: (i) $SU(2)_L \times SU(2)_2 \times U(1)_X \to SU(2)_L \times U(1)_Y$ (BP-I); (ii) $SU(2)_1 \times SU(2)_2 \times U(1)_Y \to SU(2)_L \times U(1)_Y$ (BP-II); (iii) $SU(3)_L \times U(1)_X \to SU(2)_L \times U(1)_Y$. The SM symmetry is further broken at the electroweak scale. We consider several new physics models which can be classified by the symmetry breaking pattern: (i) the left-right (LR), leptophobic (LP), hadrophobic (HP), fermiophobic (FP) models; (ii) the un-unified (UU) model and the nonuniversal (NU)model, (iii) $G(331)$ model with $\beta = \pm\sqrt{3}$ and $\beta = \pm 1/\sqrt{3}$. The phenomenology of W' and Z' bosons in the above NP models is explored at the LHC Run-1. All the decay modes of W'/Z' are included, e.g., $W' \to jj/t\bar{b}/\ell\nu/WZ/WH$ and $Z' \to \ell\ell/\nu\nu/jj/t\bar{t}/WW/ZH$.

First, we examine the possibility of interpreting the WZ excess as a 2 TeV W' boson in those NP models. The parameter spaces compatible with the experimental data are summarized in Table II. For those $G(221)$ models, a large $s_{2\beta}$ is favored to induce a large branching ratio of $W' \to WZ/WH$. For illustration we choose $s_{2\beta} \sim 1$ in Table II. In the left-right model the parameter of $0.68 \le c_\phi \le 0.81$ is compatible with both the WZ excess and $WH/jj/tb/e\nu$ upper limits, but it predicts 2.47 TeV $< M_{Z'} <$ 2.94 TeV which is in contradiction with the WW excess around 2 TeV. In the leptophobic model the parameter of $0.68 < c_\phi < 0.81$ satisfies the WZ excess and all other experimental bounds, but it predicts 2.47 TeV $< M_{Z'} <$ 2.94 TeV which is also in contradiction with the WW excess around 2 TeV. It is still difficult to judge whether or not the WW excess exists at the moment. If the 2.6σ deviation in the WW pair turns out to be from the fluctuation of the SM backgrounds, then the 3.4σ excess in the WZ pair can be interpreted as the W' boson in both left-right and leptophobic models. In the hadrophobic and fermiophobic models the production cross section of W' is too small to explain the WZ excess. In the un-unified model, we require $\Gamma_{W'} \le 0.1 M_{W'}$ to validate the NWA which yields $0.47 < c_\phi < 0.96$. The parameter of $0.72 < c_\phi < 0.73$ could address on the WZ excess and the

TABLE II. The parameter space of c_ϕ obtained from the processes of $pp \to W' \to XY$ at the LHC Run-1 in various $G(221)$ models. The W' mass is fixed to be 2 TeV. In the $G(221)$ model with BP-I, $M_{Z'} \simeq M_{W'}/c_\phi$ and $s_{2\beta} \sim 1$. The $G(331)$ models are not shown as they do not exhibit the W'-W-Z and W'-W-H couplings. The symbol × means no parameter space compatible with the current experimental limits. The symbol √ means all the parameter spaces are allowed.

		WZ	WH	$e\nu$	tb	jj	NWA	$M_{W'} \simeq M_{Z'}$
$G(221)$ (BP-I)	LR	(0.68, 0.9)	(0, 0.88)	√	(0, 0.91)	(0, 0.81)	√	(0.95, 1)
	LP	(0.68, 0.9)	(0, 0.88)	√	(0, 0.91)	(0, 0.81)	√	
	HP	×			√			
	FP	×			√			
$G(221)$ (BP-II)	UU	(0.64, 0.73)	(0.65, 1)	(0, 0.18)	(0.54, 1)	(0.72, 1)	(0.47, 0.96)	√
	NU	(0.65, 0.73)	(0.66, 1)	(0.9, 1)	√	(0.72, 1)	(0.45, 0.95)	

TABLE III. The parameter space of c_ϕ obtained from the processes of $pp \to Z' \to XY$ at the LHC Run-1 in various $G(221)$ models. The Z' mass is fixed to be 2 TeV. In the $G(221)$ model with BP-I, $M_{W'} \simeq c_\phi M_{Z'}$. Shown in the $G(331)$ models is the parameter space of α. The symbol $\times$ means no parameter space compatible with the current experimental limits. The symbol $\surd$ means all the parameter space is allowed by the current data.

		WW	ZH	ee	tt	jj	NWA	$M_{W'} \simeq M_{Z'}$
$G(221)$ (BP-I)	LR	(0.9, 0.95)	(0, 0.95)	$\times$	(0.16, 0.88)	(0.13, 0.91)	(0.23, 0.96)	(0.9, 1)
	LP	(0.89, 0.95)	(0, 0.95)	(0.99,1)	(0.13, 0.88)	(0.1, 0.91)	(0.29, 0.96)	
	HP	$\times$	$\surd$	$\times$	(0.66, 1)	(0.44, 1)	(0.34, 0.99)	
	FP	$\times$	$\surd$	(0.95, 1)	(0.6, 1)	(0.39, 1)	(0.38, 1)	
$G(221)$ (BP-II)	UU	(0.54, 0.67)	(0.53, 1)	(0, 0.19)	(0.72, 1)	(0.64, 1)	(0.47, 0.96)	$\surd$
	NU	(0.55, 0.67)	(0.55, 1)	(0.89, 1)	(0, 0.67) (0.86, 1)	(0.63, 1)	(0.45, 0.95)	
$G(331)$	$\beta = -\frac{1}{\sqrt{3}}$	$\times$	$\surd$	$\times$		$\surd$		Not Applicable
	$\beta = +\frac{1}{\sqrt{3}}$	$\times$			$\surd$			
	$\beta = -\sqrt{3}$	(−0.16, 0.16)	(−0.15, 1)		$\times$		$\surd$	
	$\beta = +\sqrt{3}$	(−0.2, 0.11)	(−1, 0.11)		$\times$		$\surd$	

$WH/tb/jj$ limits, but it comes into conflict with the tight constraint from the $e\nu$ mode ($c_\phi < 0.18$). A similar result also holds for the nonuniversal model. It is hard to explain the WW excess in the un-unified and nonuniversal models unless one can extend the models to introduce a mechanism to reduce the leptonic decays of the Z' boson. In the $G(331)$ model, the W'-W-Z and Z'-Z-Z couplings are forbidden by symmetry, therefore, it does not affect the W' phenomenology at all.

Second, we examine the possibility of interpreting the WW excess as a 2 TeV Z' boson in those NP models. The parameter spaces compatible with the experimental data are summarized in Table III. In the left-right model we require $\Gamma_{Z'} \leq 0.1 M_{Z'}$ to validate the NWA which yields $0.23 < c_\phi < 0.96$. The parameter of $0.9 \leq c_\phi \leq 0.95$ could satisfy the WW excess and ZH limit at the 95% confidence level. It has a tension with the jj mode which demands $0.13 < c_\phi < 0.91$ but predicts too large cross section of $pp \to Z' \to e^+e^-$ to respect the current experimental bound. A similar result is found in the leptophobic model. In the hadrophobic and fermiophobic models, the WW excess cannot be explained due to the small production cross section of Z'. In the un-unified model the parameter of $0.64 < c_\phi < 0.67$ satisfies the WW excess and the ZH/jj mode but is in conflict with the ee/tt mode. In the nonuniversal model the parameter of $0.63 < c_\phi < 0.67$ is compatible with the WW excess and the $ZH/tt/jj$ limits but it violates the ee limit. However, if one extend the current models to decrease the branching ratio of the Z' leptonic decays, it is still possible to explain the WW excess in the $G(221)$ models except the hadrophobic and fermiophobic models.

In the $G(331)$ models the Z'-W-W and Z'-Z-H couplings arise from the Z-Z' mixing which leads to a rich Z' phenomenology. We note that the choice of $\beta = \pm 1/\sqrt{3}$ cannot produce an enough cross section of Z' production to explain the WW excess. The parameter of $-0.17 < \alpha < 0.19$ for $\beta = -\sqrt{3}$ and of $-0.23 < \alpha < 0.12$ for $\beta = +\sqrt{3}$ could explain the WW excess and satisfy the ZH limit. However, the parameter space cannot satisfy the $ee/tt/jj$ limits.

In summary, we study in this work several new physics models with the simple non-Abelian extension of the gauge structure, either $SU(2)_1 \times SU(2)_2 \times U(1)_X$ or $SU(3)_C \times SU(3)_L \times U(1)_X$. We note that one can explain the excesses in these new physics models if either the branching ratios of the leptonic and dijet modes in the un-unified and nonuniversal model could be reduced to satisfy the experimental bounds, or the WW excess is found to be only a fluctuation of the backgrounds rather than the signal of a 2 TeV Z' in the left-right and leptophobic model.

ACKNOWLEDGMENTS

We thank Jiang-Hao Yu and Hao Zhang for useful discussions. The work is supported in part by the National Science Foundation of China under Grant No. 11275009.

APPENDIX: DECAYS OF V' (W' AND Z')

For completeness, we present the analytical expression of the partial decay width of W' and Z' bosons. The partial decay width of $V' \to \bar{f}_1 f_2$ is

$$\Gamma_{V' \to \bar{f}_1 f_2} = \frac{M_{V'}}{24\pi} \beta_0 \left[(g_L^2 + g_R^2)\beta_1 + 6 g_L g_R \frac{m_{f_1} m_{f_2}}{M_{V'}^2} \right] \Theta(M_{V'} - m_{f_1} - m_{f_2}), \tag{A1}$$

where

$$\beta_0 = \sqrt{1 - 2\frac{m_{f_1}^2 + m_{f_2}^2}{M_{V'}^2} + \frac{(m_{f_1}^2 - m_{f_2}^2)^2}{M_{V'}^4}},$$
$$\beta_1 = 1 - \frac{m_{f_1}^2 + m_{f_2}^2}{2M_{V'}^2} - \frac{(m_{f_1}^2 - m_{f_2}^2)^2}{2M_{V'}^4}. \tag{A2}$$

The color factor is not included and the top quark decay channel only opens when the Z' and W' masses are heavy.

The partial decay width of $V' \to V_1 V_2$ is

$$\Gamma_{V' \to V_1 V_2} = \frac{M_{V'}^5}{192\pi M_{V_1}^2 M_{V_2}^2} g_{V'V_1V_2}^2 \beta_0^3 \beta_1 \Theta(M_{V'} - M_{V_1} - M_{V_2}), \tag{A3}$$

where

$$\beta_0 = \sqrt{1 - 2\frac{M_{V_1}^2 + M_{V_2}^2}{M_{V'}^2} + \frac{(M_{V_1}^2 - M_{V_2}^2)^2}{M_{V'}^4}},$$
$$\beta_1 = 1 + 10\frac{M_{V_1}^2 + M_{V_2}^2}{2M_{V'}^2} + \frac{M_{V_1}^4 + 10M_{V_1}^2 M_{V_2}^2 + M_{V_2}^4}{M_{V'}^4}. \tag{A4}$$

The partial decay width of $V' \to V_1 H$ (where $V_1 = W$ or Z boson and H is the lightest Higgs boson) is

$$\Gamma_{V' \to V_1 H} = \frac{M_{V'}}{192\pi} \frac{g_{V'V_1H}^2}{M_{V_1}^2} \beta_0 \beta_1 \Theta(M_{V'} - M_{V_1} - m_H), \tag{A5}$$

where

$$\beta_0 = \sqrt{1 - 2\frac{M_{V_1}^2 + m_H^2}{M_{V'}^2} + \frac{(M_{V_1}^2 - m_H^2)^2}{M_{V'}^4}},$$
$$\beta_1 = 1 + \frac{10M_{V_1}^2 - 2m_H^2}{2M_{V'}^2} + \frac{(M_{V_1}^2 - m_H^2)^2}{M_{V'}^4}. \tag{A6}$$

Assuming the W' and Z' only decay to the SM particles, then the total decay width of the W' boson is

$$\Gamma_{W',\mathrm{tot}} = 3\Gamma_{W' \to \bar{e}\nu} + 2N_C \Gamma_{W' \to \bar{u}d} + N_C \Gamma_{W' \to \bar{t}b} + \Gamma_{W' \to WZ} + \Gamma_{W' \to WH}, \tag{A7}$$

while the width of the Z' boson is

$$\Gamma_{Z',\mathrm{tot}} = 3\Gamma_{Z' \to \bar{e}e} + 3\Gamma_{Z' \to \bar{\nu}\nu} + 2N_C \Gamma_{Z' \to \bar{u}u} + 3N_C \Gamma_{Z' \to \bar{d}d} + N_C \Gamma_{Z' \to \bar{t}t} + \Gamma_{Z' \to WW} + \Gamma_{Z' \to ZH}, \tag{A8}$$

where $N_C = 3$ originates from summation of all possible color quantum number.

[1] G. Aad *et al.* (ATLAS Collaboration), arXiv:1506.00962.
[2] V. Khachatryan *et al.* (CMS Collaboration), J. High Energy Phys. 08 (2014) 173.
[3] V. Khachatryan *et al.* (CMS Collaboration), J. High Energy Phys. 08 (2014) 174.
[4] V. Khachatryan *et al.* (CMS Collaboration), arXiv:1506.01443.
[5] H. S. Fukano, M. Kurachi, S. Matsuzaki, K. Terashi, and K. Yamawaki, Phys. Lett. B **750**, 259 (2015).
[6] J. Hisano, N. Nagata, and Y. Omura, Phys. Rev. D **92**, 055001 (2015).
[7] D. B. Franzosi, M. T. Frandsen, and F. Sannino, arXiv:1506.04392.
[8] K. Cheung, W.-Y. Keung, P.-Y. Tseng, and T.-C. Yuan, arXiv:1506.06064.
[9] B. A. Dobrescu and Z. Liu, Phys. Rev. Lett. **115**, 211802 (2015).
[10] J. Aguilar-Saavedra, J. High Energy Phys. 10 (2015) 099.
[11] Y. Gao, T. Ghosh, K. Sinha, and J.-H. Yu, Phys. Rev. D **92**, 055030 (2015).
[12] A. Thamm, R. Torre, and A. Wulzer, Phys. Rev. Lett. **115**, 221802 (2015).
[13] A. Alves, A. Berlin, S. Profumo, and F. S. Queiroz, J. High Energy Phys. 10 (2015) 076.
[14] K. Hsieh, K. Schmitz, J.-H. Yu, and C.-P. Yuan, Phys. Rev. D **82**, 035011 (2010).
[15] E. L. Berger, Q.-H. Cao, C.-R. Chen, and H. Zhang, Phys. Rev. D **83**, 114026 (2011).
[16] Q.-H. Cao, Z. Li, J.-H. Yu, and C.-P. Yuan, Phys. Rev. D **86**, 095010 (2012).
[17] P. Frampton, Phys. Rev. Lett. **69**, 2889 (1992).
[18] F. Pisano and V. Pleitez, Phys. Rev. D **46**, 410 (1992).
[19] G. Aad *et al.* (ATLAS Collaboration), Phys. Rev. D **91**, 052007 (2015).
[20] V. Khachatryan *et al.* (CMS Collaboration), Phys. Rev. D **91**, 052009 (2015).
[21] G. Aad *et al.* (ATLAS Collaboration), Phys. Lett. B **743**, 235 (2015).
[22] V. Khachatryan *et al.* (CMS Collaboration), arXiv:1506.03062 [Phys. Rev. D (to be published)].
[23] G. Aad *et al.* (ATLAS Collaboration), Phys. Rev. D **90**, 052005 (2014).
[24] V. Khachatryan *et al.* (CMS Collaboration), J. High Energy Phys. 04 (2015) 025.
[25] G. Aad *et al.* (ATLAS Collaboration), J. High Energy Phys. 09 (2014) 037.
[26] V. Khachatryan *et al.* (CMS Collaboration), Phys. Rev. D **91**, 092005 (2015).

[27] R. Mohapatra and J. C. Pati, Phys. Rev. D **11**, 2558 (1975).
[28] R. N. Mohapatra and J. C. Pati, Phys. Rev. D **11**, 566 (1975).
[29] R. N. Mohapatra and G. Senjanovic, Phys. Rev. D **23**, 165 (1981).
[30] V. D. Barger, W.-Y. Keung, and E. Ma, Phys. Rev. D **22**, 727 (1980).
[31] V. D. Barger, W.-Y. Keung, and E. Ma, Phys. Rev. Lett. **44**, 1169 (1980).
[32] H. Georgi, E. E. Jenkins, and E. H. Simmons, Phys. Rev. Lett. **62**, 2789 (1989).
[33] H. Georgi, E. E. Jenkins, and E. H. Simmons, Nucl. Phys. **B331**, 541 (1990).
[34] X. Li and E. Ma, Phys. Rev. Lett. **47**, 1788 (1981).
[35] E. Malkawi, T. M. Tait, and C.-P. Yuan, Phys. Lett. B **385**, 304 (1996).
[36] H.-J. He, T. M. Tait, and C.-P. Yuan, Phys. Rev. D **62**, 011702 (2000).
[37] R. S. Chivukula, H.-J. He, J. Howard, and E. H. Simmons, Phys. Rev. D **69**, 015009 (2004).
[38] R. S. Chivukula, B. Coleppa, S. Di Chiara, E. H. Simmons, H.-J. He, M. Kurachi, and M. Tanabashi, Phys. Rev. D **74**, 075011 (2006).
[39] E. L. Berger, Q.-H. Cao, J.-H. Yu, and C.-P. Yuan, Phys. Rev. D **84**, 095026 (2011).
[40] C. Du, H.-J. He, Y.-P. Kuang, B. Zhang, N. D. Christensen, R. S. Chivukula, and E. H. Simmons, Phys. Rev. D **86**, 095011 (2012).
[41] T. Abe, N. Chen, and H.-J. He, J. High Energy Phys. 01 (2013) 082.
[42] X.-F. Wang, C. Du, and H.-J. He, Phys. Lett. B **723**, 314 (2013).
[43] Q.-H. Cao, B. Yan, J.-H. Yu, and C. Zhang, arXiv:1504.03785 [Phys. Rev. D (to be published)].
[44] S. Patra, F. S. Queiroz, and W. Rodejohann, arXiv:1506.03456.
[45] S. Dulat, T. J. Hou, J. Gao, M. Guzzi, J. Huston *et al.*, arXiv:1506.07443 [Phys. Rev. D (to be published)].
[46] E. L. Berger and Q.-H. Cao, Phys. Rev. D **81**, 035006 (2010).
[47] H.-L. Lai, M. Guzzi, J. Huston, Z. Li, P. M. Nadolsky, J. Pumplin, and C.-P. Yuan, Phys. Rev. D **82**, 074024 (2010).
[48] A. J. Buras, F. De Fazio, and J. Girrbach-Noe, J. High Energy Phys. 08 (2014) 039.
[49] A. J. Buras, F. De Fazio, J. Girrbach, and M. V. Carlucci, J. High Energy Phys. 02 (2013) 023.
[50] L. D. Ninh and H. N. Long, Phys. Rev. D **72**, 075004 (2005).
[51] R. Martinez and F. Ochoa, Phys. Rev. D **86**, 065030 (2012).
[52] J. C. Montalvo, G. R. Ulloa, and M. Tonasse, Eur. Phys. J. C **72**, 2210 (2012).
[53] A. Alves, E. R. Barreto, and A. Dias, Phys. Rev. D **84**, 075013 (2011).
[54] J. Cieza Montalvo, N. V. Cortez, and M. Tonasse, arXiv:0812.4000.
[55] J. Cieza Montalvo, N. V. Cortez, and M. Tonasse, Phys. Rev. D **78**, 116003 (2008).
[56] J. Cieza Montalvo, N. V. Cortez, and M. Tonasse, Phys. Rev. D **77**, 095015 (2008).
[57] D. Soa, D. Thuy, L. Thuc, and T. Huong, J. Exp. Theor. Phys. **105**, 1107 (2007).
[58] D. Van Soa and D. Le Thuy, arXiv:hep-ph/0610297.
[59] J. Cieza Montalvo, N. V. Cortez, J. Sa Borges, and M. D. Tonasse, Nucl. Phys. **B756**, 1 (2006).
[60] D. Van Soa, P. V. Dong, T. T. Huong, and H. N. Long, J. Exp. Theor. Phys. **108**, 757 (2009).
[61] Y. Coutinho, V. Salustino Guimares, and A. Nepomuceno, Phys. Rev. D **87**, 115014 (2013).
[62] R. Martinez and F. Ochoa, Phys. Rev. D **80**, 075020 (2009).
[63] E. Ramirez Barreto, Y. D. A. Coutinho, and J. Sa Borges, Eur. Phys. J. C **50**, 909 (2007).
[64] E. Ramirez Barreto, Y. D. A. Coutinho, and J. Sa Borges, arXiv:hep-ph/0605098.
[65] Y. D. A. Coutinho, P. Queiroz Filho, and M. Tonasse, Phys. Rev. D **60**, 115001 (1999).
[66] A. Alves, E. R. Barreto, A. Dias, C. de S. Pires, F. S. Queiroz, and P. S. R. da Silva, Eur. Phys. J. C **73**, 2288 (2013).
[67] J. Ruiz-Alvarez, C. de S. Pires, F. S. Queiroz, D. Restrepo, and P. Rodrigues da Silva, Phys. Rev. D **86**, 075011 (2012).
[68] C. Kelso, C. A. de S. Pires, S. Profumo, F. S. Queiroz, and P. S. Rodrigues da Silva, Eur. Phys. J. C **74**, 2797 (2014).
[69] E. R. Barreto, Y. Coutinho, and J. S. Borges, Phys. Rev. D **88**, 035016 (2013).